THE ORIENTATION AND SIZES OF MOLECULAR CLOUDS IN THE GALAXY

Thesis by

Russell Ormond Redman

In partial fulfillment of the Requirements

for the Degree of

Doctor of Philosophy

California Institute of Technology

Pasadena, California

1982

(submitted November 3, 1981)

ACKNOWLEDGEMENTS

I would like to thank my advisor, Peter Wannier, for the support and encouragement he has given me over the years. Special thanks must also go to Tom Phillips who has been extremely generous with the use of the InSb receiver. I would like to thank Mark Morris for introducing me to the problem of the cloud size distribution. I have had many helpful discussions with Al Wootten, Jill Knapp, Bob Leighton, and Tom Kuiper on various aspects of radio astronomy. The friends I have found at Caltech have made the past seven years rewarding and exciting well beyond the scientific aspects.

I would like to acknowledge the support of the I have received from Caltech in the form of Tuition Scholarships for each year I have been here, as well as Research and Teaching Assistantships. I would also like to acknowledge the receipt of a National Research Council of Canada Postgraduate Scholarship during my first four years at Caltech.

ABSTRACT

In Part I of this dissertation, a technique is introduced to investigate the shapes and orientations of of molecular clouds. The clouds are shown to be roughly bar-shaped with their long axes normally aligned within thirty degrees of the axis of the spiral arm in which the cloud is embedded. The long axis is typically three times longer than the two shorter axes, although all axial ratios from one to five appear to be present. These results appear to be independent of cloud size over the range from 15 parsecs to 175 parsecs for the maximum apparent cloud dimension.

In Part II, the size distribution of the CO clouds is measured. Most of the mass of molecular gas in the galaxy resides in the largest clouds, with semimajor axes slightly larger than 100 pc long. The largest cloud sizes appear to be about the same over the entire molecular disk. These very large clouds must have been formed full sized from the intercloud gas, since they cannot have been assembled from smaller clouds. In deriving this distribution a simple and effective technique was developed to resolve the kinematic distance ambiguity.

The concentration of the mass of molecular gas into the largest clouds, and the alignment of the clouds along the spiral arms, both indicate that the clouds are very young. They must be formed directly from the intercloud medium, probably behind a

spiral arm shock wave, and cannot grow over long periods of time from smaller clouds. The mechanism forming the clouds from the intercloud gas must have a prefered scale length. Examples of such mechanisms are the Parker magnetic instability, or the collapse of a slowly accumulating dust lane. Similarly, the clouds must be dispersed rapidly at the ends of their lives.

TABLE OF CONTENTS

PART I: THE ALIGNMENT OF MOLECULAR CLOUDS

INTRODUCTION

The shapes of molecular clouds provide valuable clues about their origins and evolution. In this chapter, a technique is introduced which relates the shapes of the clouds to their galactic surroundings. The clouds will be shown to be bar-shaped with their long axes aligned parallel to the spiral arms in which they are embedded. Most of the clouds have extremely chaotic small scale structure. It is not too difficult to understand why the clouds should have ragged outlines, considering the clumpiness and turbulence of the surrounding interstellar medium and the violent activity acompanying star formation. That the clouds retain any large scale structure testifies to either the strength of the forces maintaining the structure, or the youth of the clouds, which might form with a regular structure and then be disrupted. It is difficult, however, to find any mechanism which will distort the equilibrium shape of a cloud into a bar with a fixed orientation in space. Consequently, the discussion of this chapter will consider mostly processes relevant to young, rapidly evolving clouds.

METHOD

The data used in this chapter consist of a sample of 31 clouds drawn from the literature (Baran 1978, Blitz 1978, Cong 1977, Elmegreen et al 1979, Kutner et al 1977, Lada et al 1978,

and Sargent 1977). The sizes of the clouds range from 15 parsecs to 175 parsecs. This total sample was broken into two subsets with the maximum cloud dimension either less than or greater than 40 parsecs. The two subsets contained 13 and 18 clouds respectively, enough to test whether the size of a cloud affects its shape or alignment.

The geometry of the clouds was investigated primarily using the tilt angle τ defined in Figure 1. The cloud boundaries were defined as the lowest published contours in order to study the entire cloud, not simply those regions illuminated by hot stars. The alignment of the clouds along the galactic plane implies that most of the observed values of τ lie closer to 0° than to 90°. The angle τ is not seriously affected by small irregularities on the cloud edges, except when the cloud is nearly round. Clouds which are nearly round or which are randomly oriented will have values of τ distributed uniformly between 0° and 90°. Most of the clouds used here have been completely mapped. The incompletely mapped clouds are usually truncated along their longest axis which should not greatly affect τ.

The apparent axial ratio r, defined in the caption for Figure 1, is an approximate measure of the shape of the clouds. The quantity r is more sensitive than τ to the lumps and prongs on the edges of the clouds. Since a bump of a given size will cause a larger relative increase in d than in D, these irregularities will probably cause r to be underestimated. Although r is often poorly determined, its distribution function can be used to strengthen

other results.

The viewing angle α, defined in Figure 2, was used to investigate the relation between the molecular clouds and the spiral arms in which they are embedded. The geometry assumed for the spiral arms is due to Bok (1959). However, most models for the local spiral structure are basicly similar, with Perseus, Local, and Sagitarius arms running roughly parallel to each other at an angle nearly perpendicular to the direction of the galactic center. The alignment noted in this paper is not sensitive to the particular geometry assumed, nor even to the assumption that the clouds are physically related to the spiral arms. Since the assumed spiral arms usually have small pitch angles, the main conclusion of this paper could be rephrased to say that most of the clouds are elongated along the galactic plane roughly perpendicular to the direction of the galactic center. In the few cases where the pitch angle is not small, however, the alignment works better if the spiral arms are used.

Figure 3 shows τ plotted versus α for the two samples of clouds. For $\alpha > 30^{\circ}$ almost all the measured values of τ are $< 30^{\circ}$. Therefore, the clouds typically extend farther along a spiral arm than they do perpendicular to the galactic plane. For $\alpha < 30^{\circ}$ the measured values of τ are distributed fairly uniformly between 0° and 90°. Since the apparent sizes of the clouds perpendicular to the plane should be independant of α, this requires that the clouds are more extended along the spiral arms than in either of the perpendicular directions, ie. the clouds

are roughly bar-shaped and cannot be disks. This is important since many of the mechanisms which could be shaping the clouds would flatten the clouds into disks. Furthermore, we note that the long axes of the clouds are constrained to lie within 30° of the axis of the spiral arm.

Although all of the major conclusions of this paper can be drawn using Figure 3 alone, the distribution of r with α, shown in Figure 4, can be used as a consistancy check for the results. Notice that the measured values of r tend to be smaller for $\alpha \leq 30°$ than for $\alpha > 30°$. For example, 81% of the clouds with $\alpha \leq 30°$ have $r \leq 2$, while 67% of the clouds with $\alpha > 30°$ have $r > 2$. This is the behavior expected for a collection of aligned bars, which should appear foreshortened when seen end on. To check that the degree of forshortening is reasonable, the clouds were modelled as an ensemble of prolate spheroids. In keeping with the observed alignment, the long axes of the spheroids were constrained to lie within 30° of the plane of the Galaxy, and the projections of the axes onto the plane were constrained to lie within 30° of a fixed line representing the axis of the spiral arm. For simplicity, the axial ratios of all the spheroids were assumed to be the same. Note that the full distribution function $R(r,\alpha)$ cannot be estimated from the data since it is not possible to guess the number $N(\alpha) \equiv \int_1^\infty R(r,\alpha)dr$ of clouds which would be expected at each value of α. To compare the model to the data it is necessary to use the relative distribution

$$p(r|\alpha) \equiv R(r,\alpha)/N(\alpha)$$

The behavior of r with α can then be seen by defining the 20 and 80 percentile points of the cumulative distribution

$P(r|\alpha) \equiv \int_1^r p(s|\alpha)ds$

as the functions $L(\alpha)$ and $U(\alpha)$, ie.

$P(L(\alpha)|\alpha) = .2$

$P(U(\alpha)|\alpha) = .8$

Details of the computation of $P(r|\alpha)$ from the model are given in the appendix. The curves $L(\alpha)$ and $U(\alpha)$ are also shown in Figure 4 for an intrinsic axial ratio of 3. Axial ratios of 2.5 and 3.5 were also tried, but the resulting curves did not follow the data as well. Although one cloud has an apparent axial ratio greater than 4, and several of the clouds with large values of α have apparent axial ratios near 1, $U(\alpha)$ provides a good upper bound, and $L(\alpha)$ provides a fair lower bound, for most of the points in the figure. The observed foreshortening indicates that an axial ratio of 3 is typical for most of the observed clouds, although all ratios from one to five seem to be present.

One of the more striking features of Figures 3 and 4 is that the samples of small and large clouds are well mixed. There are no statistically significant differences in the distributions of the clouds in either tilt angle or axial ratio. For example, for $\alpha \geq 30^\circ$ the ratio of the number of clouds with $\tau \geq 30^\circ$ to those with $\tau \leq 30^\circ$ is 2:6 for the large clouds and 2:5 for the small clouds. Apparently, the factors which control the cloud shapes and alignments do not change significantly over an order of magnitude in the linear size of the clouds. It would be useful to

strengthen this curious result with a larger sample of small clouds.

DISCUSSION

There are only a few simple processes which could make bar-shaped molecular clouds. It is easy to discount centrifugal force as a major factor in the shape of the clouds. It is possible that the tidal shear of the galaxy could be pulling the clouds apart. It seems quite clear that the galactic magnetic field plays some role at least in the small scale structure of the clouds, although it is less obvious how it may affect the large scale structure studied here. Passage of a cloud through a spiral shock wave would have complicated and dramatic effects upon the shape of the cloud. Finally, star formation must have dramatic effects on the structure of the clouds. In the following paragraphs these topics will be briefly discussed.

Chandrasekar (1969a) has shown that a uniform, self-gravitating ellipsoid is subject to the growth of a bar-like instability if its axial ratio is larger than 1.72. Since the observed axial ratios are almost all greater than 1.72, we might expect the clouds to be bar-shaped. However, the clouds would be seen at random phases in their rotational periods. Because the clouds are more extended along the arms than they are perpendicular to the plane, the rotation axis would have to be perpendicular to the plane. That, however, would imply that τ should be small for all viewing angles α, contrary to the

observations.

Also, the radial velocity structure of the clouds often does not show rotation. For example, neither the Cep OB 3 molecular cloud (Sargent, 1977) nor the Ser OB 1 cloud (Elmegreen et al, 1979) show large velocity gradients. Linke and Wannier (1974) interpret the velocity gradient of the Ori OB 1 cloud as rotation. Kutner et al. (1977), however, observe that the motion could have been started by the radiation pressure of the OB associations which have recently formed from the cloud. Motion induced in this way must be transient and will not result in a balance between the self-gravity of the cloud and the centrifugal force, if only because the cloud will soon be consumed by the ongoing star formation.

Another large scale force which could quite easily produce bar-shaped clouds is the tidal shear of the galaxy. For a fluid of uniform density with no internal motions orbiting a point mass Chandrasekar (1969b) has shown that the equilibrium configuration is a triaxial ellipsoid whose longest axis points towards the central mass. In the Galaxy this would stretch the clouds nearly perpendicular to the observed direction. It is likely, however, that the stretching is much more complex than this, since the clouds are surrounded by hot, turbulent gas and are threaded with magnetic fields. Stark and Blitz (1978) have analyzed the tidal disruption of clouds in the Galaxy, concluding that the shear can explain the apparent cutoff in the sizes of molecular clouds at around 100 parsecs if the maximum mass is $\leq 5 \times 10^5 M_\odot$. Considering

the large axial ratios of the clouds, many of them may be only marginally bound gravitationally. Such clouds could not have collapsed under their own self-gravity from a less dense state. Nongravitational forces, such as magnetic instabilities, the spiral shock wave, or intercloud collisions, must be invoked to create the clouds. Once assembled, the clouds might prove to be unstable and might shear from the differential rotation of the Galaxy into filaments and bars.

The problem of the cloud dynamics in the interstellar magnetic field is very complex. Cohen et al. (1980) discuss in some detail how the Parker instability (Parker, 1966) might collect dense H I clouds into large complexes. Appenzeller (1974) suggests that the Ori OB 1 cloud now sits in a 'magnetic pocket', and that the pocket and cloud may have formed together in a Parker instability. A similar structure is seen more clearly near Per OB 3 (Appenzeller, 1971), and Vrba (1977) interprets the magnetic fields around ρ Oph (Vrba et al, 1976) in the same way. Furthermore, where the gas forms long, thin filaments the magnetic field often runs parallel to the filaments (Vrba et al, 1976, Elmegreen and Elmegreen, 1978). It is clear that magnetic fields and molecular clouds are intimately related. Notice, however, that sitting in a magnetic pocket would shorten the clouds along the direction of the magnetic field. Since the mean magnetic field runs parallel to the spiral arms (Heiles, 1976), the magnetic pocket model does not seem to explain the elongation of the clouds parallel to the arms. On the other hand, once the gas

has been collected, it will move most easily along the magnetic field lines, so that clouds created in some other way might become bar-shaped and aligned parallel to the spiral arms as they try to disperse. More studies of the magnetic fields in the vicinity of molecular clouds are needed to clarify this important issue.

Cohen et al. (1980) have shown that molecular clouds are fairly well concentrated into spiral arms. Entry into a spiral arm may then be the event triggering cloud formation. There are several ways this might happen. Roberts (1969) has shown that a sufficiently cool interstellar gas will develop a strong shock wave as it passes into a spiral arm. Woodward (1978) has investigated numerically the passage of an interstellar H I cloud through such a shock and concludes that it is easily possible to compress the cloud to high densities in this way. The initial effect of passage through a shock front is a strong flattening of the cloud into a disk parallel to the front. This flattening may help to orient the resulting molecular clouds parallel to the shock front, although as the H I cloud in the model fragmented, the fragments expanded into filaments perpendicular to the shock front. Many difficult problems remain in determining whether the shock even exists, what the effect of frozen-in magnetic fields might be, how the gas is collected into large molecular clouds behind the shock, and so forth. It is at least suggestive that the molecular clouds appear to be oriented parallel to the predicted shock front.

Star formation is probably the most spectacular factor affecting the cloud shapes. The long chains of OB associations which trail away from many molecular clouds (Blaauw, 1964) may indicate the former sizes of the clouds. Alternately, Elmegreen (1979) has suggested that the clouds are temporarily dispersed and accelerated by the star-making activity, and will recondense again some distance away. Yet another possibility, suggested by Norman and Silk (1980), is that the formation of T Tauri stars in the dense parts of molecular clouds may provide a source of turbulent pressure capable of supporting the clouds against gravitational collapse. This might allow other forces weaker than the self-gravity of the cloud to control the shape, but does not suggest what they might be. It is difficult to see how any of these mechanisms could shape the clouds into bars aligned with the spiral arms. Also, large parts of the Ser OB 1 and Ori OB 1 molecular clouds lie far away from the regions of prominent star formation, appearing optically as dark dust lanes. Although spectacular, star formation does not appear to be responsible for the clouds being extended along the spiral arms.

It is interesting to compare molecular cloud shapes to the shapes of the optical dark nebulae. These also appear to be elongated along the galactic plane, but Disney and Hopper (1974) concluded that they were disk-shaped rather than bar-shaped. They concluded that the elongation of the optical dark nebulae was due to the gravitational field of the stellar disk, flattening the clouds along an axis perpendicular to the plane. The density of a

molecular cloud, however, is at least ten times larger, and often hundreds of times larger, than the mean density of matter in stars in the galactic plane. The slight gravitational background of the stars should not significantly affect the shapes of the molecular clouds. It is possible, however, that the disk-shaped dust clouds become bar-shaped molecular clouds when they pass through a spiral shock wave and are compressed.

CONCLUSIONS

Molecular clouds seen in the nearby spiral arms have, on the average, a barlike shape. The long axes of the clouds are normally aligned within 30° of the axis of the spiral arm in which they are embedded. It is likely that all axial ratios from one to five are present among the clouds, with an axial ratio of three being typical. There does not appear to be any significant difference in this respect between small clouds whose maximumum linear size ranges from 15-40 parsecs and large clouds whose maximum sizes range from 40-175 parsecs. The alignment of the clouds is probably a dynamic effect which may involve the tidal shear of the galaxy, the galactic magnetic field, and possibly the galactic spiral shock wave.

PART II: THE SIZE DISTRIBUTION OF MOLECULAR CLOUDS IN THE GALAXY

INTRODUCTION

The CO(1-0) transition was first observed by Wilson, Jefferts, and Penzias (1970) in the direction of the Orion nebula. After the initial detection in Orion, other H II regions and dark nebulae were examined, and it soon became clear that CO is a major constituent of the dust clouds which are the breeding places of stars. It also became clear that CO is widely distributed throughout the galaxy. The CO is generally confined to discrete, cold clouds, referred to as molecular clouds because of their rich chemistry. Some of the largest clouds occur in the galactic center. Separated from these by a large, almost empty annulus lie the molecular clouds of the galactic disk. The latter clouds, which are the object of this study, are found mainly from 4 kpc to 8 kpc from the galactic center, and are confined to a thin layer in the galactic plane with a scale height near 50 pc (Solomon et al 1979).

Since the molecular clouds are so intimately related to the dust clouds and OB associations which delineate the spiral structure of other galaxies, an understanding of the origin, lifetimes, and ultimate fate of the clouds will be necessary before we can understand completely either star formation or the spiral structure of galaxies. For example, Solomon et al (1979) have suggested that the clouds are very long-lived and dominate the mass of the interstellar medium between 4 and 8 kpc from the galactic center. If so then the most natural way to make large

molecular clouds would be to have small clouds stick together when they collide. The clouds would continue to grow until star formation or some other disruptive event broke them back into smaller clouds. Since the clouds could not be confined to spiral arms, this could explain the raggedness of the spiral structure seen in many galaxies. As has been shown by Kwan (1979) and Cowie (1980) this model would require the presence of a large number of small clouds from which the large clouds could be assembled. An alternate model would suggest that the clouds have very short lifetimes. They would then have to be regenerated directly from the intercloud medium, probably behind a spiral shock wave where the gas would be unstable against gravitational collapse (see, for example, Elmegreen, 1979) or the Parker instability (Blitz and Shu 1980). Dynamic instabilities such as these have preferred scale lengths, so that many of the clouds would have about the same size. It is possible to distinguish between these two models by measuring the size distribution of the clouds. The results reported in this chapter show that there are too many large clouds for them to have grown from the existing population of small clouds. In fact, nearly all of the clouds observed at high resolution were too large to fit completely into the observing grids. Furthermore, the largest clouds have a characteristic size which is nearly constant over the entire molecular disk. Together these observations provide clear evidence that the largest clouds must be formed directly from the intercloud gas and suggests that the smaller clouds are primarily fragments produced during the collapse of larger clouds.

There were three major steps to measuring the size distribution of the clouds, each of which will be dealt with in a separate section of this chapter. Firstly, as many as possible of the clouds in a suitably chosen region of the galactic plane were identified and mapped. This provided a collection of 145 objects. Secondly, the distances of the clouds were estimated. For most of the clouds the only available distance estimator is the kinematic distance, which provides two possible distances for each velocity. A major effort was made to resolve the ambiguity between these two possible distances. In the final step, the measured angular sizes and distances of the clouds were combined with an estimate of the biases in the observing technique to deduce the true size distribution. The observational bias was estimated using a model of the clouds as a set of ellipses in the plane of the sky overlapping the grid of observations. From the model it was possible to estimate the probabilty for each cloud that it would have the observed size. The maximum likelihood method was then used to find the optimal size distribution.

THE CLOUD MAPS

Introduction

It is relatively simple to map most molecular clouds. They generally have simple spectra, consisting of a single sharp peak several kilometers per second wide. Liszt (1973) has shown that the radial velocity does not change very much across the width of

most molecular clouds. So long as the clouds do not crowd too close together in velocity, they can be mapped by simply following the emission peaks in the spectra from one position to the next. Only in two places was there evidence for complex, possibly self-absorbed line profiles. The principle complication was that, although the mean velocity did not vary by much across most clouds, the velocity width and peak temperature could change dramatically from one point to the next. These variations, plus the individual judgments required to resolve blended features into individual clouds, prevented any attempt to automate the cloud mapping process. In particular, the clouds could not be mapped reliably by making maps of the mean emission in fixed velocity ranges.

The following three subsections will discuss the instrumentation and observational techniques used, the choice of the observing grids, and the criteria used to identify and map each cloud. The fourth subsection will explain the actual statistic used to measure the cloud sizes, and will describe in detail Table 1 which lists all of the observed clouds and their properties.

Instrumentation and Observational Methods

The first dish of the Owens Valley Radio Observatory Millimeter Interferometer was completed in the winter of 1977. After a period in which the first attempts were made to understand the pointing of the telescope, an InSb receiver (Phillips and

Jefferts, 1973) was mounted on the telescope in March 1978. This receiver provided a single data channel 1 MHz wide with a system temperature typically in the range 250°K to 400°K. At the CO(2-1) frequency (230,538 MHz) the telescope provided a main beam 26" in diameter. I used this receiver in a mapping mode where the central frequency was held fixed and the telescope beam was swept across the source. In March 1979 an uncooled Schottky diode mixer receiver was mounted on the telescope. This receiver, operating at the CO(1-0) frequency (115,271 MHz), was used with the 1024 channel autocorrelator for the bulk of the observations in the large grid. (The division of the data into observing grids is discussed below.) At this frequency the main beam was almost exactly 1' in diameter. Effective single sideband system temperatures, including the signal loss in the autocorrelator, were typically between 3000°K and 4000°K. The autocorrelator passband was slightly more than 40 MHz wide. With this receiver and backend it was usually possible to get an acceptable signal to noise on 12 points in a strip across the galactic plane in a single night. On good nights two such strips could be completed. In the summer of 1980 the second dish of the interferometer was completed and the first dish was taken out of service for repairs and modifications. In December 1980 and January 1981 an SIS receiver (Woody et al., 1981), also operating at CO(1-0), was mounted on dish two for an extended observing run. An acousto-optical spectrometer (Masson, 1980) was used for the backend, providing a 100 MHz passband in 512 channels. The single sideband system temperature was typically around 400°K. This

receiver and backend were used to complete the large grid and to observe all of the smaller grids.

The data were calibrated using an ambient temperature absorber and an absorber soaked in liquid nitrogen as temperature references. The opacity of the atmosphere was measured by observing how the antenna temperature varied as the telescope was moved from the zenith to near the horizon. The spillover factor was typically 10% for the first dish and 15% for the second dish. The main beam efficiency, as measured by comparing the antenna temperature of Jupiter or Venus with that for the center of the moon, was 55% for point sources and was the value used during data reduction. Position switching was used to subtract the baselines for all of the CO(1-0) data. It was normally possible to map with the InSb receiver in total power. If the weather did not permit this, frequency switching was used to stablize the signal.

Baseline removal was initially a problem for the CO(1-0) data taken with the room temperature receiver because thermal cycling in the receiver box changed the shape of the passband on timescales as short as 5-10 minutes. This was cured partially by insulating the receiver, and partially by processing the spectra in groups through a program which removed the largest variations in the shape of the spectra. This procedure worked very well if only small clouds were encountered in each set of spectra. Very large clouds, however, were liable to be confused with part of the receiver gain variation. Because of this, some large clouds may be larger in b than they appear.

The Observing Grids

To measure the size of a cloud, it is necessary to map the cloud in both l and b. Strip maps along the galactic plane can measure only a cross section through the cloud and will almost always underestimate the size of the cloud. Clouds with complex shapes might cross the strip in several places, exaggerating the apparent numbers of small clouds in the map. In addition, the next section will show how the distribution of the clouds in galactic latitude can effectively resolve the kinematic distance ambiguity. Finally, the observing bias against small clouds is much less serious for a well sampled grid than for a strip map. For these reasons I chose to map the CO(1-0) emission on the largest possible grid of points in the galactic plane, rather than map strips along or across the galaxy.

The choice of which region of the galaxy to observe was guided by the need to measure the sizes of as many clouds as possible, as accurately as possible. It is easiest to observe large numbers of clouds in the molecular ring. To measure the kinematic distances of the clouds accurately, the cloud velocities should be spread over the widest possible range. These two conditions are admirably met near $l = 25°K$ where the line of sight is roughly tangential to the inner edge of the molecular ring. Near the tangential velocity, however, the clouds will crowd together in velocity, becoming difficult to distinguish. This problem can largely be avoided by observing the region $l \leq 25$, since in this region the tangential points lie inside the inner

edge of the molecular ring where the density of clouds is much smaller. Finally, the survey by Gordon and Burton (1976) indicated that the majority of the clouds would lie below the galactic plane. With these considerations in mind, I chose to map the clouds in the region $20 \leq l \leq 26$, $-1.5 \leq b \leq 0.5$.

Since it is not possible to map such a large region with 1' resolution in a reasonable time, the CO(1-0) observations were broken into four overlapping grids. The separation between observed points in each grid was the same in l and b. The largest grid filled the entire region with a spacing of 12' between points. This grid was capable of mapping clouds up to 1 kpc in linear size at the distance of the galactic center, but could not resolve any cloud smaller than 35 pc at the same distance. The smaller grids, whose relation to the 12' grid is shown in Figure 5, had separations of 4', 2' and 1' between points, allowing me to resolve clouds down to 3 pc at the distance of the galactic center. The nearest clouds observed lay 150 pc from the sun. At that distance the smallest potentially observable cloud would be only .05 pc across, although no such clouds were observed. With this set of grids I could measure the cloud size distribution over 4.5 orders of magnitude.

The CO(2-1) data were also taken on a grid, except that this grid consisted of completely mapped lines instead of spectra, usually two degrees long and centered on b = -0.5°K, at l = 20°K, 21°K, 22°K, 23°K, 24°K, 25°K, and 26°K, and at V_{LSR} = 30, 40, 50, and 60 km s^{-1}. I had intended to compare these with the CO(1-0)

data to show the run of optical depth, and therefore density, across the cloud. This would have been an important step in linking the size distribution of the clouds to their mass distribution. Unfortunately, because of the baseline subtraction problem mentioned above, the CO(1-0) data were not good enough for the comparison to be useful. This should be rectified in the near future, and has no direct effect on the rest of the project.

The Mapping Technique

I considered that a cloud was certainly present where a clearly distinguishable peak in the spectrum had a maximum temperature greater than 4°K. From these warm spots the boundaries of the cloud were extended to adjacent points until the peak temperature dropped below 3°K or until an abrupt change in the velocity of the peak by more than a few kilometers per second indicated that a physical boundary had been reached. In some velocity ranges, parts of most of the cloud boundaries were obscured by blending with other clouds, but the disputes could often resolved by the assumption of constant cloud velocity.

Figure 6 illustrates the procedure with a section of the 4' grid covering the velocity range from 0 to 50 km s^{-1}. The peak to peak noise is about 1°K, so most of the bumps in the figure are real features. The shaded region in each spectrum was attributed to a single cloud whose mean velocity was 25 km s^{-1}. The cloud is clearly present at (12,4), (12,0), (0,4), and (-4,8) with peak temperatures greater than 4°K. Additional points at 3°K can be

seen at (12,-4), (8,4), (4,8), and (-4,4), joining the warmer spots and extending the boundaries slightly. Table 2 gives a more complete analysis of the cloud, showing that it is not a great deal larger than the 3°K boundary even if very weak possible extentions are included. The line is blended in several places with another line centered at 21 km s^{-1}, but even there can be distinguished as a separate bump at 25 km s^{-1} on the wing of the larger feature. The tip of this cloud can be seen in the 1′ grid. It has not been detected in the 12′ grid, indicating that its maximum size is likely less than ~30′. Notice that if the size of this cloud had been measured from a set of points along the galactic plane, only the single point on the extreme left of the figure would have been detected, without even a suggestion of the true extent of the cloud, stretched over 20′ in the bounds of this figure.

Specification of the Cloud Sizes

I chose to measure the size of a cloud by counting the number of grid points at which the cloud was observed, referred to as the AREA in Table 1. This is a simple estimator of the angular area of the cloud and is the quantity most closely related to the volume (and hence mass) of the cloud. Several other measures of cloud size were also considered, but were rejected as less useful. For example, the maximum angular separation of any two points in the cloud is the most obvious measure of its size, but does not distinguish large fat clouds from smaller, but long and thin,

clouds. Another possibility is to take moments around the center of the cloud, which might be useful in studies of the cloud dynamics if the density distribution in the cloud were also known. The moments are excessively complicated to compute, however, and can only be found for clouds which are completely contained within one of the observing grids. By contrast, the AREA statistic is easy to measure and is fairly easy to model for clouds which only partly overlap the observing grid.

Table 1 lists all of the clouds observed in the four grids. The first column, labelled ID, gives the identification of the cloud in the form of a running number assigned in order of increasing velocity and increasing right ascension, followed by a colon and the grid spacing in minutes of arc. The second column, labelled VLSR, indicates the mean velocity of the cloud, or the range of velocities where that was appropriate. The third column, labelled AREA, gives the number of points in the grid at which the cloud was observed. The fourth column, labelled C/E, indicates whether the cloud was completely contained within the center of the grid (C), or whether it overlapped the edge of the grid (E). The fifth column, labelled N/F indicates whether the cloud was certainly at the near kinematic distance (N), probably at the near kinematic distance (N?), probably at the far kinematic distance (F?), or certainly at the far kinematic distance (F). This classification will be discussed in more detail in the section on kinematic distances. The sixth column, labelled $\langle l \rangle$, gives the mean galactic longtitude of the cloud. The seventh column,

labelled r, gives the apparent axial ratio for those clouds observed at more than four points. This quantity is defined for irregular shapes in the section on calculating the size distribution. The last column, labelled COMMENTS, indicates whether the cloud was observed on more than one grid. If so, the alternate ID of the cloud in the other grids is given. To avoid multiple counting of a cloud which was observed on several grids, only the observations on the grid which most accurately measured the cloud size were used. The alternate identifications are flagged in the COMMENTS column with an asterisk, and were ignored in the remainder of the analysis. Also, because the velocity coverage in the 12′ grid does not extend uniformly above 100 km s^{-1}, any clouds with velocities greater than 100 km s^{-1} were also flagged with an asterisk and ignored.

DETERMINATION OF KINEMATIC DISTANCES

Introduction

The kinematic distance is the only available estimate of the distance for most clouds. In the next subsection, the formulae used to compute the kinematic distance are summarized, and some of the potential sources of error are discussed. The two subsections following that discuss two methods to resolve the kinematic distance ambiguity. The first, and by far the most successful, uses the fact that the clouds are confined to a thin layer in the galactic plane. Thus most of the clouds on the far side of the

galaxy are confined to a narrow band of galactic latitude, within which they normally outnumber clouds on the near side by a large factor. As a byproduct of finding this range of latitude, it is also shown that the thickness of the molecular disk is virtually constant across the entire galaxy. Furthermore, density structures which can tentatively be identified as spiral arms have been found. In the second method, the locations of the clouds were examined for evidence of H I absorption. An absorption feature produced by cold H I on the far side of the galaxy would likely be substantially filled in by emission from gas on the near side. Thus, when absorption was seen, the cloud was considered likely to be nearby. This method was not sufficiently reliable to be used by itself, but provided a useful confirmation of the first method.

Of the 145 clouds detected in this survey, it was possible to assign unambiguous kinematic distances to 90. The remaining 55 clouds usually had large radial velocities. Near the tangential velocity the difference between the NKD and the FKD is small, making the angular thickness of the disk nearly the same for both distances. The galactic latitude method therefore usually fails. Because of the velocity crowding near the tangential velocity, the H I absorption method also fails. Fortunately, because the ratio of the NKD to the FKD is close to 1, it does not matter as much if an error is made. Even when it was not possible to assign a cloud to either distance with much certainty, it was possible to give a probability for each distance. I broke the clouds up into four

groups labelled N, N?, F?, and F, in which the probability that the cloud was at the FKD was 0, 1/3, 2/3, and 1, respectively (see Table 1).

Basic Kinematic Distance Considerations

Since the derivations of the kinematic distance formulae are well known, only the results are reproduced here. If we can assume that the clouds are moving on circular orbits around the galactic center, then the radial velocity of a cloud at galactic longtitude 1 gives the distance of the cloud from the galactic center directly from the formula

$$R = 1.03-X+[(1.03-X)^2+7.93]^{1/2} \quad (1)$$

where $X = V_{1sr}/(32.4 \sin 1)$. Equation (1) is based on an approximation due to Burton (1971) of the circular rotational velocity measured by Shane and Bieger-Smith (1966) for the range 4 kpc $\leq R \leq$ 10 kpc. I have also assumed that the sun lies 10 kpc from the galactic center. Knowing R and 1, there are two possible kinematic distances for the cloud, the near kinematic distance (NKD) at

$$D_1 = 10 \cos 1 - (R^2 - 10 \sin^2 1)^{1/2} \quad (2a)$$

and the far kinematic distance (FKD) at

$$D_2 = 10 \cos 1 + (R^2 - 10 \sin^2 1)^{1/2}. \quad (2b)$$

Throughout this section, quantities which may be different at the two distances will be denoted with a subscript 1 for the NKD value and subscript 2 for the FKD value. Occasionally the subscript will be dropped when there is no confusion about which value is

meant.

In addition to the circular motion around the galaxy, there are streaming motions in the gas, and peculiar velocities for each cloud. These noncircular motions have typical amplitudes around 10 km s^{-1}. They can seriously affect the value of D_1, but have relatively little effect on D_2. It is likely, therefore, that the estimated sizes of the nearest clouds are in error by 20% or even 50%. Fortunately, there are only a few clouds near enough for this to be a serious problem, so this source of error should not affect the measured distribution significantly.

Resolution of the Kinematic Distance Ambiguity Using the Distribution of the Clouds in Galactic Latitude

If the density of clouds in the galaxy were a function only of the distance from the galactic center, then within the range of b where both the near side and the far side of the disk are visible, the clouds on the far side would outnumber those on the near side by a factor of $(D_2/D_1)^2$. The first method therefore seeks a range of galactic latitude $[b_{min}(v), b_{max}(v)]$ which is a function of velocity such that any cloud lying within the range is almost surely on the far side of the galaxy, and any cloud extending beyond the range is almost surely on the near side of the galaxy.

For this purpose it is adequate to assume that the number density of molecular clouds varies across the thickness of the disk as a gaussian. The angular density of the clouds as a function of galactic latitude will then be the sum of two gaussians corresponding to the two kinematic distances detectable at each longtitude l and velocity v:

$$\rho(b) = N_1 \text{ EXP } -\frac{1}{2}\left[\frac{b-B_1}{W_1}\right]^2 + N_2 \text{ EXP } -\frac{1}{2}\left[\frac{b-B_2}{W_2}\right]^2 \qquad (3)$$

In equation 3, N_1, B_1, W_1 and N_2, B_2, W_2 represent the total number of clouds across the thickness of the molecular disk, the mean galactic latitude of the disk, and the angular width of the molecular disk at the near kinematic distance (subscript 1) and the far kinematic distance (subscript 2) respectively. Except when N_2 was so much smaller than N_1 that the clouds on the far side of the galaxy never dominated those on the near side, $[b_{min}(v), b_{max}(v)]$ was usually taken to be $[B_2-W_2, B_2+W_2]$.

To determine the parameters of the gaussians, each spectrum was broken into 10 km s^{-1} intervals, starting at 0 km s^{-1}. Within each interval, the fraction f(l,b,v) of the interval occupied with emission stronger than 2°K was measured, where (l,b) are the coordinates of the point and v is the velocity at the middle of the interval. To improve the signal to noise f was averaged over each degree, resulting in a set of functions $\langle f_{l,v}(b) \rangle$ which

measure the fraction of the sky covered by the clouds as a function of galactic latitude for each degree along the sky and each 10 km s^{-1} velocity interval. Since it is not possible to cover more than 100% of the sky, the saturation of the coverage was taken into account by fitting $1-\exp[\rho(b)]$ to $\langle f_{l,v} \rangle$. The resulting coefficients are shown in Tables 3, 4, and 5.

It is possible to check that the measurements described above are yielding reasonable results. The product WD should be a measure of the thickness of the molecular disk at the distance D. Because the disk has a fairly uniform thickness (Solomon et al, 1979), this quantity should be independant of the distance D. The quantity N is a direct measure of the amount of molecular gas at the distance D. Because the matter in the molecular gas is organized into spiral arms (Cohen et al, 1980), the largest values of N should lie in bands in Table 5. The bands should be most prominent on the far side of the galaxy since a larger number of clouds will contribute to each of the N(l,v). Finally, the product BD is a measure of the displacement of the molecular disk from the plane of the galaxy. Although there is no theory or observations to indicate what reasonable behavior would be for B, it would be intuitively satisfying if B varied slowly and smoothly along the spiral arms. The following three paragraphs will show that all of these predictions are confirmed by the data in Tables 3, 4, and 5. (Notice that it is not useful to make a map of the galaxy with the data described here because of the small range of galactic longtitude covered and because the important

inner regions of the galaxy with radial velocities above 100 km s^{-1} were not observed.)

Although the linear thickness of the disk, corresponding to the standard deviation of the gaussian, is given directly by the product WD, I chose in Figure 7 to plot W, the observed angular thickness, against 1/D, which is proportional to the predicted angular thickness of a disk with a constant linear thickness. The mean linear thickness of the disk is given by the slope of the best fitting line through the origin. The estimated thickness using least squares is 44 $\pm$ 11 pc. The molecular disk appears to have a remarkably uniform thickness across the entire galaxy. The scatter in the measurements is mostly due to the relatively small number of clouds observed in each cut across the galactic plane. When only a single cut is used instead of averaging $\langle f \rangle$ over a full degree of longtitude, the plane typically appears much narrower and B has a correspondingly larger scatter. Averaging over more than a degree does not increase the estimated size significantly. In conclusion, the angular widths do appear to measure the thickness of the molecular disk at the expected kinematic distance.

Deciding on the internal consistancy of the mean displacements B from the galactic plane requires a brief consideration of the density structure in the plane. Table 4 shows the measured values for N(1,v). As has been previously mentioned, N_1 was poorly determined for $v < 40$ km s^{-1}. The large number of nearby clouds, and the relative paucity of distant ones,

made N_2 poorly determined for $v < 10$ km s^{-1}. In Table 4 all the points above these two velocity limits which have $N \geq 0.15$ have been outlined. This region fills most of the available space in the N_1 table and extends in a long sloping arm from $l = 25.4°K$, $v = 115$ km s^{-1} to $l = 21.4°K$, $v = 35$ km s^{-1}. A second feature in the N_2 table seems to run from $l = 25.4°K$, $v = 45$ km s^{-1} to $l = 21.4°K$, $v = 15$ km s^{-1}, roughly parallel to the first. I have tentatively identified these high density regions as spiral arms. Regardless of their interpretation, they appear to be physically related regions.

The same regions are outlined in Table 5, which lists the measured values of B. As expected, most of the estimates of B are negative, especially in the outlined regions which include most of the emission. Closer inspection reveals that B_1 becomes less negative towards larger galactic longtitudes, and higher velocities, ultimately becoming positive above 90–100 km s^{-1}. Correspondingly, B_2 starts out slightly positive at high velocities, and becomes more negative as the galactic longtitude and velocity decrease along the main "spiral arm". It is less clear what happens along the second "spiral arm", but B_2 appears to be mostly positive in this region. $|B|$ rarely exceeds 2W anywhere in the table. Although large jumps in B do exist, (notably between $l = 23.5$ and $l = 24.4$ at $v = 65$) they are unusual. Mostly, B varies smoothly along the "spiral arms". Outside of the "spiral arms", B is poorly measured. The estimates tend either to be similar to those measured nearby in the "spiral

arms" if the density is still modest, or to scatter around zero if the density is too low.

In summary, the widths of the gaussians are consistant with their representing a layer of fairly uniform thickness across the entire galaxy, and the displacements from the galactic plane are consistant with smooth, simple undulations along the "spiral arms" tentatively identified in Table 4. The clouds within the range $[B_2-W_2, B_2+W_2]$ can be considered to lie at the far kinematic distance with considerable confidence.

Resolution of the Kinematic Distance Ambiguity Using H I Absorption Features at 21 CM

To confirm the assignment of NKD or FKD to each of the molecular clouds, their locations were examined in the Maryland-Greenbank 21 cm survey of the galactic plane (Westerhout, 1973) for evidence of H I absorption. This was motivated by the observation that some nearby molecular clouds have extensive cold H I envelopes visible as absorption features at 21 cm (see, for example, Sato et al. 1980). In the 12′ grid, similar absorptions were found at 4 km s^{-1} and 10 km s^{-1}, coincident with two large sets of molecular clouds. Although the H I absorptions cover the entire region, the CO clouds are generally weak and patchy, as has also been noticed by Kazes and Crovisier, 1980. Absorption profiles would only be expected for relatively nearby clouds, since the absorptions of more distant clouds would be partially filled in by emission from intervening warm gas. In practice, the

presence or absence of absorption was only a weak indicator of the distance of a cloud. Clouds considered to be distant because of their galactic latitude generally did not show absorption, as expected, but neither did many clouds outside the critical range of latitude. Such clouds would not show any absorption unless a warm cloud lay behind them with the same radial velocity, an unlikely event if the cold cloud lies somewhat out of the plane. Those clouds which did show probable absorption features were mostly larger objects overlapping the critical range of latitude. Since most of them were large, they had already been assigned the near kinematic distance. It was reassuring, however, to check that there was not a class of tremendously large clouds lurking on the far side of the galaxy.

CALCULATION OF THE CLOUD SIZE DISTRIBUTION

Introduction

The data in Table 1 require careful interpretation if the correct size distribution is to be found. Like most surveys, this one is heavily biased towards large clouds. Also, many of the clouds, especially the very largest, overlap the edges of the grids so that their true size is unknown. However, if the true size distribution can be approximated by a function with a fixed number of parameters, then it is possible to calculate for each set of parameters the probability that a cloud of a particular size will be found in the center or on the edge of an observing

grid, using a model of the observations. The size distribution can then be estimated by maximizing the likelihood of the observed cloud sizes.

This section will describe the process in detail. The first subsection will introduce the maximum likelihood method and will show how a histogram is a maximum likelihood estimator for a distribution in the absence of observational bias. This subsection will also indicate how the biases can be taken into account. The second subsection will discuss the known sources of bias in this set of data. The third subsection will discuss the model used to estimate the observational biases. Finally, the last subsection will report on the actual size distribution measured from the data in Table 1.

The Maximum Likelihood Method

To introduce the maximum likelihood method, consider a simpler problem in which there is no observational bias. Suppose a sample (v_i) has been taken of a random variable in the interval [a,b] with the density distribution V. The likelihood of the sample is defined as

$$L = \sum_i V(v_i) \tag{4}$$

If the distribution V depends upon a finite and fixed set of unknown parameters, then the maximum likelihood estimate of the parameters is that set which maximizes L. For example, break the interval [a,b] into N subintervals $x_n < x_{n+1}$, $x_0 = a$, $x_{N+1} = b$,

with length $q_n = x_{n+1} - x_n$ and approximate the density distribution V with a sum of box functions, ie.

$$V(x) = V_n \tag{5}$$

on $[x_n, x_{n+1}]$, with

$$C = \sum_n V_n q_n = 1. \tag{6}$$

Then equation 4 becomes

$$L = \sum_i V_n^{k_n} \tag{7}$$

where k_n counts the number of v_i in the interval $[x_n, x_{n+1}]$, and L should be maximized subject to the constraint in equation 6. It is more convenient in this case to maximize ln(L). Applying the method of Lagrangian multipliers,

$$\partial/\partial V_m(\ln(L) - \lambda C) = k_m/V_m - \lambda q_m. \tag{8}$$

Solving for V_m and substituting in equation 6

$$\lambda = \sum_n k_n \tag{9}$$

which gives finally

$$V_m = \frac{k_m}{q_m} \frac{1}{\sum_n k_n}. \tag{10}$$

Notice that V_m is proportional to k_m and inversely proportional to q_m, ie. the maximum likelihood estimate of the distribution V is a simple histogram in the absence of observational bias.

When there is a known observational bias in the data, a similar procedure can be used if the bias is included explicitly in the definition of the likelihood. Each observation must be treated as coming from a different probability distribution

$Y_i(V_j, O_k, v)$ in which some of the parameters (O_k) are known from the observations and some (V_j) parameterize the unknown, intrinsic distribution of the variable. The unknown parameters can be estimated by maximizing the logarithm of the biased likelihood

$$\ln(L) = \sum_i \ln[Y_i(V_j, O_k, v_i)] \qquad (11)$$

with respect to the (V_j).

Known Sources of Bias

There are six sources of bias inherant in this set of data. The statistical model which will be developed in the next subsection corrects for problems (i) through (iv). Problem (v), the kinematic distance ambiguity, has been dealt with already. The last problem can be resolved by careful consideration of the shapes of the observed clouds. This is done in the next subsection.

i) Large clouds can overlap the grids from farther away than small clouds. The seriousness of this effect has been minimized by making the 12′ grid as large as practically possible, but it remains the largest single effect distorting the observed distribution.

ii) Many small clouds are missed between the points of the larger grids. This effect is especially important for distant clouds which might be missed even when they are quite large. The separation of the observing points in the 12′ grid is ~70 pc at a distance of 20 kpc allowing clouds with semimajor axes as large as 105 pc to be missed.

iii) The linear diameter of the telescope beam increases proportionally with distance from 0.05 pc at 150 pc (the distance to the nearest major collection of clouds) up to 6 pc at 20 kpc. Clouds whose semimajor axes are smaller than half the diameter of the main beam normally cannot be seen.

iv) All of the clouds were incompletely mapped. It was possible to make a complete map of a cloud only in the 1′ grid, and all of the clouds observed in that grid overlap the edge of the grid by an unknown amount. Even in the centers of the larger grids, there is a range of possible sizes for each of the observed clouds.

v) The ambiguity in the kinematic distance has been discussed above. The most common mistake made in previous attempts to measure the size distribution of the clouds has been to assume that all of the clouds were at the near kinematic distance. This had the effect of greatly overestimating the numbers of small clouds in the distribution.

vi) Real clouds have very complex shapes. Some care must be taken when interpreting their angular areas in terms of linear sizes.

It is possible to estimate how serious problem (ii) is by noting that 11 of the 22 objects mapped in the 4′ grid with velocities less than 90 km s^{-1} were not seen in the 12′ grid. Since some of the groups of edge clouds seen in the 4′ grid are undoubtedly the edges of large clouds just bordering the grid, the degree of undercounting is likely less than a factor of 2 overall. Furthermore, there are very few clouds completely contained in the centers of the small grids. Partly this is due to the sizes of

the grids, in a 7x7 grid such as the 1' grid or the 4' grid, 24 of the 49 points lie on one of the edges. Mostly, however, it is because the clouds are too large to fit within the grids. There are only 2 center clouds out of 28 objects in the 4' grid, 6 out of 40 in the 2' grid, and none at all in the 1' grid. If the size distribution of the clouds were a steeply sloping power law, a large population of clouds should have been present, each occupying a single point of the grid. Even at this stage it is clear that no such population exists.

A Model of the Observations

To handle these sources of bias, a model of the cloud sizes, shapes, and spatial distribution was developed. The observed data for each cloud were the velocity of the cloud, the angular area of the cloud, the probability that the cloud was at the far kinematic distance, the grid in which the cloud was observed, and a flag indicating whether the cloud was completely contained within the grid or spilled over the edge. From the measured velocity, the size of the observing grid, and the probability that the cloud was at the FKD, the model computed the probability Y that the cloud would cover the observed number of points in the center or on the edge of the grid. The following paragraphs will explain the details of the model and how this probability was calculated.

The clouds were modelled as a collection of ellipses on the plane of the sky. The ellipses were all assigned an axial ratio of 3. The tilt angles τ of the major axes were assumed to be randomly distributed between 0° and 90°. The centers of the ellipses were constrained to lie within 44 pc of the galactic plane at the appropriate kinematic distance, and were assumed to be uniformly distributed in b within this constraint. The centers were assumed to be uniformly distributed in l at each velocity. The observing grid was included in the model as a grid of points centered on the galactic plane. An ellipse was considered to have been observed at a point in the grid if that point lay in the interior of the ellipse. An ellipse could be specified uniquely by the four numbers (l,b,τ,A) giving the coordinates of the center, and the tilt angle and length of the semimajor axis of the ellipse. (Notice that the SEMImajor axis was used to measure the size of the ellipse. The quoted sizes for the observed clouds are also half-sizes, corresponding to the radii and not to the diameters of the clouds.) The probability Y(N,CE,GRID) that that ellipse will be observed at N points in the center or on the edge (logical variable CE) of the grid (GRID) is therefore proportional to

$$V(N,CE,GRID) = \int K(N,CE,GRID,A)N(A)dA \qquad (16)$$

where K(N,CE,GRID,A), the volume kernal, is the volume of (l,b,τ) space in which this condition is met for clouds with semimajor axis A, and N(A) is the probability density of cloud sizes as a function of A. The normalizing factor was the sum $\sum_{N}\sum_{CE}\sum_{GRID} V(N,CE,GRID)$ and could be expressed as a similar integral

whose kernal $K_T(A) = \sum_N \sum_{CE} \sum_{GRID} K(N,CE,GRID,A)$ will be referred to as the normalizing kernal. Thus, Y(N,CE,GRID) could be computed as

$$Y(N,CE) = \int K(N,CE,GRID,A)N(A)dA / \int K_T(A)N(A)dA \qquad (17)$$

The axial ratios and orientations of the ellipses in this model have been chosen to be consistant with the observation in Part I of this dissertation that the molecular clouds in the nearby spiral arms are bar-like objects whose typical axial ratios are 3:1. I have modified the definition of "axial ratio", however, to be more appropriate in the current context. The new definition directly relates the area of the cloud to its total length. Defining the separation of two points in the cloud as the length of the shortest path joining the points without passing outside the boundary of the cloud, the total length X of the cloud may be defined as the largest separation between two points in the cloud. The axial ratio can in turn be defined as $r = \pi(X/2)^2/AREA$, where AREA is the measured area of the cloud. It is easy to see that this is equivalent to the usual definition for elliptical clouds. When applied to the 36 clouds seen in the 12′ grid which cover 5 or more points, the mean axial ratio is 3.8. This likely overestimates the mean apparent axial ratio of the clouds since those clouds seen end on have both smaller axial ratios and smaller angular areas, and may have been systematically excluded from the average. An axial ratio of 3 appears to be a simple and reasonable estimate of the true average.

In Part I it was observed that the clouds in the solar neighbourhood are aligned along the spiral arms so that the tilt angles are less than 30° when the clouds are seen side on. However, most of the clouds seen in these grids are fairly close to the tangential point where the spiral arms run nearly parallel to the line of sight. The clouds will therefore be seen nearly end on and will have a much larger range of tilt angles.

The volume kernal K(N,CE,GRID) is computed as the product of four terms:

$$K(N,CE,GRID) = (\int Pr(N,GRID,R)\ O(CE,GRID,R,A)\ dR)\ S(CE,GRID,A)\ Pr^{*}(GRID,A) \qquad (18)$$

where Pr(N,GRID,R) is the probability that an ellipse oriented randomly between 0° and 90° with a semimajor axis of length R will be observed at N points on an infinite square grid with the same grid spacing as GRID, O(CE,GRID,R,A) is the probability that a cloud whose semimajor axis has length A will overlap the observing grid by the area $\pi R^2/3$, S(CE,GRID,A) is the volume in (l,b,τ) space in which the cloud lies completely (CE = center) or partially (CE = edge) inside the the observing grid, and $Pr^{*}(GRID,A)$ is the probability that the cloud is not seen on two or more points in a larger grid (since its size would then be measured in the larger grid, not the smaller). Notice that $O(center,R,A) = \delta(R-A)$, so that for center clouds the integral in equation 17 simplifies to Pr(N,GRID,A). Similarly, for center clouds or for edge clouds in the 12′ grid, $Pr^{*}(GRID,A) = 1$. It might be objected that the inner integral should not use the same

function Pr(N,GRID,R) for both center clouds and edge clouds, since in the model when a large ellipse overlaps the observing grid by a small area, the overlap region will not even slightly resemble an ellipse with an axial ratio of 3. Real clouds, however, have structure on all scales, and it is likely that if a large cloud overlaps the observing region by a small amount, that small region will have a structure appropriate to a smaller cloud. This is one of the few places in this problem where nature and expediency both recommended that a simplifying approximation be made. Details of the derivations of Pr(N,GRID,R), O(edge,GRID,R,A), and S(CE,GRID,A) are given in appendix 2.

Because the sizes of the detectable clouds range over 4.5 orders of magnitude, from .03 pc up to 1 kpc, it was useful to work not with A, but with $\alpha = \log A$ in the actual computations. The α axis was broken into 9 intervals starting at $\alpha = -1.5$ and running up to $\alpha = 3$. The lengths of the intervals were chosen so that there would be roughly equal numbers of clouds in each interval. Corresponding to the logarithmic axis, the quantity computed was $\mu(\alpha) = A\,N(A)$, the probability density of cloud size on the α axis. As discussed before, μ was assumed to have a constant value μ_i in the i'th interval. By numerically evaluating the integrals in equation 17, Y(CE,GRID,N) was expressed as a rational function of the μ_i

$$Y(CE,GRID,N) = \frac{\sum_i C_i \mu_i}{\sum_i F_i \mu_i} \qquad (19)$$

If the cloud were in the classes N? or F?, then this calculation

had to be done for both of the possible kinematic distances. The final expression for Y_i was

$$Y_i = (1-p_f)Y_n + p_f Y_f \qquad (20)$$

where p_f was the the probability that the cloud was at the far kinematic distance and Y_n and Y_f indicate the expressions for the near and far kinematic distances respectively.

Figures 8 and 9 show graphically the shapes of the kernals and the values of the coefficients in the numerator and denominator of equation 17. The exponential growth of the kernal of the formalizing factor is due to the logarithmic abscissa. The normalizing kernal grows rapidly from zero up to about the area of the observing grid as A increases from half of the beam size to about twice the grid spacing. It is roughly constant until A becomes comparable to the overall size of the grid. If the observing grid is much smaller than the galactic plane at the distance of the cloud, the normalizing kernal will then grow as A^2 until A becomes comparable to the thickness of the galactic plane. After that the kernal grows roughly linearly with A up to the largest size considered. If the cloud has been observed at a large number of points in the grid, it does not matter greatly whether it was observed on the edge or in the center; in both cases the kernal of the numerator (the volume kernal) peaks fairly sharply, although it peaks at a larger size for edge clouds than for center clouds with the same area. If the cloud has been

detected at only a single point, the volume kernal spreads over a wide range of sizes. For edge clouds the same slope changes discussed for the normalizing kernal are apparent. In addition, in Figure 9c, the sudden jump in the volume kernal at $\alpha = 2.5$ happens because at that size it fairly abruptly becomes impossible to put any cloud in the center of the grid so that the entire volume formerly occupied by center clouds is suddenly added to the volume for edge clouds.

When the volume kernal is nonzero over several intervals, it introduces correlations into the estimated numbers of clouds in each bin. Basicly, the algorithm cannot decide which interval to credit with each cloud, since they are about equally likely. This is only troublesome for the three bins covering the range $0 \leq \alpha \leq 1.5$, which are dominated by the large numbers of middle sized clouds seen on the far side of the galaxy. Even there, trouble is encountered only when the the data are split into smaller samples with insufficient numbers of clouds in each interval.

Results

This subsection reports on the computed size distribution and on two tests which were conducted to check that the kinematic distance ambiguity had been successfully resolved and to see if any differences could be found between clouds in the inner galaxy and those farther out.

Figure 10 shows the derived distribution of cloud sizes using all the data in Table 1. The data are adequately fitted by a power law size distribution

$$\mu(A) \propto A^{-0.72} \tag{21}$$

over the entire range from A = .03 pc up to A = 100 pc. Above 100 pc the number of clouds falls off sharply. No clouds larger than 300 pc were seen at all.

As a check that the kinematic distance ambiguity had been successfully resolved, the clouds in Table 1 were broken into two groups containing all of the clouds in the classes N and N?, and in the classes F and F? respectively. If a significant fraction of the clouds had been misidentified, the size distribution based on F and F? would have had considerably more large clouds than the distribution based on N and N?. In fact, there were no significant differences between the distributions computed from these two groups, indicating that the classification had been fairly successful.

To see if there might be any change in the size distribution with distance from the galactic center, the data in Table 1 were separated into two roughly equal groups whose velocities were all either greater or less than 60 km s^{-1}. The resulting size distributions are given in Table 6. There appears to be a shortage of small clouds in the high velocity group, and a small excess of very large clouds. To test whether the differences between the two distributions were significant, Table 6 also lists the effective number N_i of clouds seen in each interval, which is

proportional to the product of μ_i, the width of the interval in α, and the volume of the galaxy in which a cloud of that size could have appeared in the data sample. The latter number was obtained by adding together the coefficients for all of the normalizing factors in the sample. In this way it was possible to compute for any input size distribution the number of clouds which should have been seen in each size bin of an actual data sample, automatically including the observing bias and the number of clouds observed at each distance. The effective number of clouds actually seen in the high velocity sample was compared to that predicted from the low velocity sample. Notice that the high velocity distribution cannot be used to predict the low velocity distribution, since the very small clouds seen in the low velocity sample could not be detected at the distance of even the nearest cloud in the high velocity sample. Because the N_i are correlated from bin to bin, it is not strictly valid to use Poisson statistics to test them. To reduce the degree of correlation, the worst offenders (the second, third, and fourth bins) were combined into a single bin. Clouds larger than 30 pc were large enough to be seen on several points over most of the galaxy, and the corresponding N_i are fairly independant of each other. Applying the Chi squared test to the rebinned numbers, the hypothesis that the distributions are the same can be rejected with 98% confidence. An even simpler and more robust test is to compare the ratio of the effective numbers of clouds larger than 45 pc to those smaller than 45 pc for the two distributions. Again, the hypothesis that the two distribution are the same can be rejected with 99% confidence.

Considering that some trouble should still be expected from correlations among the N_i, this is marginal evidence that the two distributions are different. It is interesting to note that four more clouds were observed at still higher velocities than are listed in Table 1. They were omitted because the spacial coverage at velocities higher than 100 km s^{-1} (the limit of the data taken with the autocorrelator) was too sparse to draw reliable maps. All four clouds detected above this velocity, however, appeared to be larger than 50 pc.

DISCUSSION

There are two striking features about the size distribution computed here. Firstly, the distribution is fairly flat, ie. there is a relatively large number of big clouds. Secondly, the cutoff in the sizes of the the largest clouds is the same over the entire molecular disk. To interpret these results, assume that the gas density inside the clouds is the same on average for all of the clouds. These two observations can then be rephrased to say that the masses of the largest clouds are the same over the entire galaxy, and that almost all of the mass in molecular form resides in the largest clouds. The extent to which the mass is concentrated into the largest clouds is shown in Figure 11, which plots the distribution of mass per logarithmic mass interval. The uppermost filled bin, containing only 0.14% of the total number of clouds, contains over 65% of the mass. The largest 3.5% of the clouds contain 99% of the mass. Small clouds may be easy to find,

but they contain a negligable fraction of the molecular gas in the galaxy.

Kwan (1979) has analysed the buildup of large molecular clouds from the collisions of smaller clouds. In the simplest models, the clouds stick together every time they collide and suffer no losses from star formation or other disruptive forces until they reach some critical size. In these models the collisional cross section and the mean velocity dispersion of the clouds were assumed to vary with mass as power laws:

$$\sigma \propto m^{a} \tag{22a}$$

$$v \propto m^{-b}. \tag{22b}$$

Since the collision cross section is essentially the projected area of the cloud and will vary as A^2, equation (22a) implies that the mass of the cloud varies with A as $m \propto A^{2/a}$. (notice that this implies that the density varies as $A^{2/a-3}$.) The resulting size distribution is

$$\mu(A) \propto A^{-\beta} \tag{23}$$

where $\beta = 1-b+1/a$. Physically plausible values of a and b, corresponding to constant density and equipartion of kinetic energy, are $a = 2/3$, $b = 1/2$, giving $\beta = 2$, much steeper than the observed distribution. Observationally, it appears that $b \sim 0$ except for the very largest clouds (Stark, 1979), increasing the discrepancy. Adding disruptive terms makes it harder for very large clouds to form, steepening the distribution even further. Another feature of the collisional accumulation model is that the largest size a cloud can attain increases roughly as the 4/3 power

of the density of matter in the smaller clouds surrounding it. Since the density of the molecular gas increases by a factor of 10 from the solar neighbourhood to the inner molecular ring, we should see a factor of 3 variation in the size of the largest clouds. Although the mean size of the clouds does seem to increase towards the galactic center, Table 6 shows that the reason is primarily a decrease in the number of smaller clouds. The distribution of the largest clouds does not change significantly. Furthermore, Elmegreen et al (1979) have shown that the largest clouds in the Sagitarius arm are just as large as any seen closer to the galactic center. It is evident that collisional accumulation of large clouds from many smaller clouds cannot account for the observed size distribution.

If large clouds cannot grow from smaller clouds, they must have been formed with their current size. The obvious mechanism for this is the gravitational collapse of a dust lane, perhaps aided by the interstellar magnetic field in a Parker instability (Parker, 1966). Elmegreen (1979) analyses this problem in some detail. In the absence of strong tidal forces, he shows that a collapsing dust lane should form clouds with a characteristic mass depending upon the local density and temperature of the H I, the thickness of the galactic plane, and the Mach number of the spiral shock wave which creates the dust lane. None of these quantities are strong functions of galactic radius in the region of the galaxy surveyed here. The suggested mechanism controlling the size is quite simple; mass accumulates in the dust lane until its

mass per unit length exceeds the critical mass for collapse. Obviously, most of the clouds will form with the characteristic size which becomes unstable first, creating a large number of clouds with about the same mass. The shock reorganizes itself as the cloud drifts off, and the dust lane begins to accumulate mass again. The resulting clouds must collapse by a large factor before CO molecules form, and possible fragmentation during this process could produce an unknown range of molecular cloud sizes. The evidence of this paper, however, is that each H I cloud likely forms a single giant molecular cloud complex whose characteristic size is 50–100 pc.

It is less obvious how this picture of cloud formation can account for the large numbers of small clouds which are also seen. It is perhaps relevant to notice that many of the smallest clouds in the sample come from the large H I–molecular cloud complexes at 4 km s^{-1} and 10 km s^{-1}. It seems plausible that most of the small molecular clouds may be fragments associated with larger H I and CO complexes. Nonetheless, it is also possible that smaller H I clouds occasionally might be directly compressed to densities large enough to form CO. It is also tempting to think that the large clouds may be broken into smaller pieces by H II regions and supernovae. The fragments, however, could not contain much of the mass of the original cloud. Alternately, they could be very short-lived, evaporating rapidly back into the ambient gas, or, following a suggestion by Elmegreen (1979), recollecting rapidly into a new giant molecular cloud. There is no room in Figure 11

for a large population of long-lived fragments.

CONCLUSIONS

The size distribution of CO clouds in the Galaxy has been measured and shown to be consistant with a power law up to a critical size of 100 pc, above which the distribution cuts off sharply. Almost all of the mass in molecular gas in the Galaxy resides in the largest clouds. It is not possible to create such clouds by collisions of smaller clouds. Instead it seems likely that the size of the large clouds is the characteristic size for the fragmentation of a dust lane behind a spiral shock front.

APPENDIX 1

If a prolate spheroid with an intrinsic axial ratio r_0 is viewed from an angle ω with respect to its major axis, it is easy to show that the apparent axial ratio r_1 will be

$$r_1 = [\, r_0^2 + (1-r_0^2)\cos^2 \omega \,]^{1/2} \tag{24}$$

Thus, the probability that $r_1 \leq r$ is the same as the probability that

$$\cos \omega \geq [(r_0^2-r^2)/(r_0^2-1)]^{1/2} \tag{25}$$

Suppose now that the spheroid is embedded in a spiral arm and that its major axis deviates from the axis of the spiral arm by an angle η perpendicular to the plane of the galaxy, and by an angle ξ parallel to the plane. As before, the observer views the cloud from an angle α with respect to the axis of the spiral arm. Basic spherical geometry then gives

$$\cos \omega = \cos(\alpha-\xi)\cos \eta \tag{26}$$

The angles η and ξ are absolutely bounded by η_0 and ξ_0. Let A_0 be the area of this rectangular region of the η-ξ plane and $A(r,\alpha)$ be the area inside the rectangle for which

$$\cos(\alpha-\xi)\cos \eta \geq [(r_0^2-r^2)/(r_0^2-1)]^{1/2} \tag{27}$$

$A(r,\alpha)$ can be evaluated numerically using a Guassian quadrature to give

$$P(r|\alpha) = A(r,\alpha)/A_0 \tag{28}$$

APPENDIX 2

Consider an ellipse whose axial ratio is r and whose semimajor axis has length A, randomly placed upon an infinite square grid of points. The separation between grid points will be taken to be unity in this appendix. Pr(N,A), the probability that N points of the grid will lie inside the ellipse, was evaluated in three different ways, depending upon A. If $A \leq 1/2$, it is clear that

$$Pr(N,A) = \begin{cases} 1-\pi rA^2, & N = 0 \\ \pi rA^2, & N = 1 \\ 0, & N \geq 2 \end{cases} \qquad (29)$$

If $A \geq 1/2$, more than one point might lie inside the ellipse. Imagine that ellipses with the same size, shape, and orientation, are placed with their centers on every one of the points in the grid. Each square of the grid would then be broken into regions with area B_i, $i = 0,\infty$, in which exactly i of the ellipses overlap. Clearly, if the center of the test ellipse is placed in the i'th region it will contain i points of the grid. It was easy to write a program to evaluate the B_i numerically. Pr(N,A) could then be evaluated by averaging B_N over all tilt angles. The probabilities were evaluated once and stored in a table for fast access. For ellipses covering more than 20 points this procedure became prohibitively slow and a simple approximation was derived. As the ellipse became larger, the distribution over N approached a normal distribution. Noticing that $\sum_i iB_i = \pi rA^2$, we see that the average number of points inside the ellipse is equal to the area of the

ellipse. The number of points which are close to the edge of the ellipse should be proportional to its circumference, so that the standard deviation of N should be proportional to $A^{1/2}$. The constant of proportionality was found by fitting a gaussian to the last column in the table computed above. This last approximation was checked by doing spot calculations for much larger ellipses. Small errors were considered tolerable in this approximation because very few clouds were large enough to use it and because the mean value of N could be calculated exactly, ensuring that the basic behavior of the approximation would be reasonable.

It is only necessary to compute O(edge,R,A) for the case in which the cloud is smaller than the size of the grid since almost all of the clouds are smaller than the sides of the 12′ grid, and the sizes of clouds which overlap the smaller grids are severely restricted by the requirement that they not be seen in the surrounding larger grid. Because of this simplification the edge of the grid can be approximated as the side of the xy plane with $x \leq 0$. If the ellipse is centered at (x,0) and is tilted at an angle τ to the y axis, it overlaps the grid region on an area

$Q = \pi r R^2 = \pi r A^2 \gamma(\xi)$ where

$\xi = (r^2\cos^2\tau + \sin^2\tau)^{-1/2}$ and

$\gamma(x) = [\cos^{-1}(x) - x(1-x^2)^{-1/2}]/\pi$. If $|x| > A\,(r^2\cos^2\tau + \sin^2\tau)^{1/2}$ the ellipse will not cross the boundary of the grid and will not be an edge cloud. The mean maximum distance from the center of the cloud to the boundary of the grid is $\langle x_{max} \rangle = A\,E(1-r^2)$, where

E is the complete elliptic integral of the second kind. The ellipses will be uniformly distributed in (x,τ) space. To compute $O(R,A)$, this uniform distribution must be transformed to (x,Q) space and averaged over x, ie.

$$O(R,A) = (\int \partial\tau/\partial Q \, dx)/(\pi\langle x_{max}\rangle)$$

where $(-x_{max}, x_{max})$ are the limits of the integral. Transforming to the dimensionless coordinates $x^* = x/A$ and $\gamma^* = Q/(\pi r A^2)$,

$$O(R,A) = (\int_{-1}^{1} 1/\pi \; \partial\tau/\partial\gamma^* \, dx^*)/[2rA^2E(1-r^2)].$$

Now $\gamma^* = \gamma(\xi)$, where $\xi = x^* (r^2\cos^2\tau + \sin^2\tau)^{-1/2}$. Thus $d\xi/d\gamma^* = -(\pi/2)\,(1-\xi^2)^{-1/2}$. Notice that this term factors out of the integral, since $\gamma(\xi) = (R/A)^2$, ie. ξ is not a function of x^*. Defining $y = x^*/\xi$,

$$\partial\tau/\partial\xi = y^2[(1-y^2)(y^2-r^2)]^{-1/2}$$

so

$$O(R,A) = (\int_r^1 y^2[(1-y^2)(y^2-r^2)]^{-1/2} dy)/[4rA^2\,E(1-r^2)(1-\xi^2)^{1/2}]$$

which gives finally

$$O(R,A) = [4rA^2(1-\xi^2)^{1/2}]^{-1} \qquad (30)$$

The derivation of S(CE,GRID,A) is very similar to the derivation of O(edge,R,A). First, the total volume in $(1,b,\tau)$ space in which the ellipse overlaps any part of the grid is calculated. This quantity is always needed to calculate the normalizing factor. Then the volume in which the ellipse lies completely inside the grid [ie. S(center,GRID,A)] is calculated. If it is needed, S(edge,GRID,A) is the difference between these two quantities.

It was shown above that the clouds will overlap the edge of the grid out to an average distance of $A\,E(1-r^2)$. If the thickness of the molecular disk is smaller than the size of the grid at the distance of the cloud, then to an adequate approximation the total volume in (l,b,τ) space in which the cloud overlaps the grid will be

$$S(total,GRID,A) = \pi B_{PL}[L(GRID) + 2\,A\,E(1-r^2)] \qquad (31)$$

where L(GRID) is the length of the grid in galactic longtitude and B_{PL} is the thickness of the galactic plane. Similarly, if the molecular disk is much larger than either the grid or the size of the cloud then the volume is given to an adequate approximation by extending the boundaries of the grid in all directions by $A\,E(1-r^2)$, ie.

$$S(total,GRID,A) = \pi L(GRID)B(GRID) + 4A\,[L(GRID)+B(GRID)]\,E(1-R^2) + \pi^2 rA^2 \qquad (32)$$

As the size of the cloud becomes comparable to the thickness of the galactic plane, equation (32) is no longer applicable. After a complex transition range, equation (31) will again become a good aproximation. For simplicity, I computed both approximations (31) and (32) and accepted the smaller of the two as an adequate approximation for S(total,GRID,A).

It was necessary to compute exactly S(center,GRID,A), the volume of (l,b,τ) space in which the ellipse occupied the center of the grid. Because the model has reflectional symmetry across the galactic plane, it is only necessary to compute the volume for $\tau \geq 0$, and then multiply by 2. The largest possible ellipse which

can fit inside the ellipse has

$$A_{max} = \{[L(GRID)^2+B(GRID)^2]/[1-r^2]\}^{1/2} \qquad (33)$$

If the ellipse is larger than A_{max} then S(center,GRID,A) = 0. For smaller clouds there are three important angles which determine the volume:

$$\tau_{max} = \begin{cases} \pi/2 & , 2A \leq B(GRID) \\ \cos^{-1}\{[(1-B(GRID)/2A)/(1-r^2)]^{1/2}\} & , A < A_{max} \end{cases}$$

$$\tau_{min} = \begin{cases} 0 & , 2A \leq L(GRID) \\ \sin^{-1}\{[(1-L(GRID)/2A)/(1-r^2)]^{1/2}\} & , L(GRID) < A < A_{max} \end{cases}$$

$$\tau_{crit} = \begin{cases} 0 & , A \geq A_{PL}/r \\ \cos^{-1}\{[(1-A_{PL}/A)/(1-r^2)]^{1/2}\} & , A_{PL} < A \leq A_{PL}/r \\ \pi/2 & , A \leq A_{PL} \end{cases}$$

where $A_{PL} = (B(GRID)-B_{PL})/2$. Then

S(center,GRID,A) =

$$= B_{PL}\{L(GRID)[\tau_{max}-\tau_{min}]-2A[E(\tau_{max},\phi_1)-E(\tau_{min},\phi_1)]\}$$
$$, \tau_{crit} > \tau_{max}$$

$$= B_{PL}L(GRID)(\tau_{crit}-\tau_{min})-2AB_{PL}[E(\tau_{crit},\phi_1)-E(\tau_{min},\phi_1)]$$
$$+L(GRID)B(GRID)(\tau_{max}-\tau_{min})-2AB(GRID)[E(\tau_{max},\phi_1)$$
$$-E(\tau_{crit},\phi_1)]-2AL(GRID)[E(\pi/2-\tau_{crit},\phi_1)-E(\pi/2-\tau_{max},\phi_1)]$$
$$+(1+r^2)A^2[E(2\tau_{max}-\pi/2,\phi_2)-E(2\tau_{crit}-\pi/2,\phi_2)]$$
$$, \tau_{min} < \tau_{crit} \tau_{max}$$

$$= L(GRID)B(GRID)(\tau_{max}-\tau_{min})$$
$$-2AB(GRID)[E(\tau_{max},\phi_1)-E(\tau_{min},\phi_1)]$$
$$-2AL(GRID)[E(\pi/2-\tau_{min},\phi_1)-E(\pi/2-\tau_{max},\phi_1)]$$
$$+(1+r^2)A^2[E(2\tau_{max}-\pi/2,\phi_2)-E(2\tau_{min}-\pi/2,\phi_2)]$$
$$, \tau_{crit} \leq \tau_{min}$$

where $\phi_1 = \cos^{-1} r$ and $\phi_2 = \sin^{-1}[(1-r^2)/(1+r^2)]$.

TABLE 1

ID	VLSR	AREA	C/E	N/F	⟨1⟩	r	COMMENTS
1:12	4-5	7	E	N	20.2	.18	
2:12	4-5	6	E	N	22.63	.66	
3:12	4-5	3	C	N	22.73	-	
4:12	4-5	1	E	N	26.0	-	
5:12	8	14	E	N	21.09	.76	
6:12	8	7	C	N	21.0	.20	
7:12	8	3	C	N	22.0	-	
8:12	8	4	E	N	23.35	-	
9:12	8	2	C	N	23.4	-	
10:12	8	1	E	N	23.4	-	
11:12	8	3	E	N	24.0	-	
12:12	8	1	C	N	24.6	-	
13:12	11	2	C	F	25.7	-	
14:12	12	2	C	F	22.3	-	
15:12	13	1	C	F	21.6	-	
16:12	14-17	4	E	F	20.4	-	
17:12	14	1	C	F	21.2	-	
18:12	15	1	E	F	24.2	-	
19:12	18	2	C	F	23.6	-	
20:12	20	1	C	N?	20.6	-	
21:12	20	4	E	N?	21.4	-	
22:12	21-22	2	C	F	22.3	-	
23:12	22	1	C	F	23.2	-	
24:12	25	1	E	F	20.2	-	
25:12	25	1	C	F	22.0	-	
26:12	25	1	C	F	23.2	-	3:1,4:4 *
27:12	26	2	E	F	20.5	-	
28:12	28	1	C	F	22.4	-	
29:12	30	1	E	F	20.2	-	
30:12	30	5	C	F	20.76	.55	
31:12	30	1	E	F	20.8	-	
32:12	30	1	C	F	21.4	-	
33:12	30	2	C	F	24.7	-	9:2
34:12	30	1	C	F	25.8	-	
35:12	34-36	1	C	F	23.4	-	4:1,9:4 *
36:12	34-36	5	C	F	24.4	.43	11:2,13:2
37:12	34-36	1	C	F	25.2	-	
38:12	35	1	C	F	22.4	-	
39:12	36	1	E	N?	20.2	-	
40:12	36	7	C	F?	20.94	.32	
41:12	38	2	C	F	21.2	-	
42:12	38	4	C	F	22.55	-	
43:12	38-40	1	C	F	23.2	-	
44:12	38-40	4	C	F	23.95	-	
45:12	42	7	E	N?	20.23	.30	
46:12	42	2	C	N?	21.0	-	
47:12	42	4	C	N?	21.6	-	
48:12	42	9	C	N?	22.4	.39	

TABLE 1 (cont.)

ID	VLSR	AREA	C/E	N/F	⟨1⟩	r	COMMENTS
49:12	42	2	C	N?	22.4	–	
50:12	42	11	E	N	24.49	.27	14:2
51:12	42	1	E	N?	26.0	–	
52:12	44–46	1	C	N	25.2	–	
53:12	44–46	4	E	N	25.5	–	
54:12	45	1	C	N?	23.2	–	
55:12	45	3	C	N	24.33	–	
56:12	47	5	C	F?	20.56	.55	
57:12	48	15	C	N?	22.45	.28	
58:12	48	7	C	N?	24.83	.26	15:2,16:2
59:12	50	7	E	F?	24.4	.26	17:2
60:12	52–55	52	E	N	22.54	.20	18:2,11:4
61:12	52–55	2	C	N?	23.4	–	
62:12	52–55	6	C	N?	25.03	.26	
63:12	52–55	7	E	N	25.03	.26	
64:12	52–55	6	E	N	25.77	.33	
65:12	52	5	E	N?	20.4	.55	
66:12	55	4	C	N?	25.35	–	
67:12	58	1	E	F?	20.2	–	
68:12	58	9	E	F?	20.78	.21	
69:12	58	7	C	F?	23.43	.26	
70:12	58	11	C	F	25.02	.30	
71:12	58	2	C	F	24.6	–	18:2
72:12	58	1	E	F	26.0	–	
73:12	62	1	E	N?	20.2	–	
74:12	62	24	E	N?	22.67	.18	10:1,12:4
75:12	62	3	C	F	24.0	–	19:2
76:12	62	14	C	F?	25.24	.19	
77:12	65	2	C	N?	22.5	–	
78:12	65	1	C	F?	25.4	–	
79:12	65–67	12	E	N	20.77	.16	
80:12	68	1	C	N	22.2	–	
81:12	68	19	C	N	22.73	.20	12:4
82:12	68	1	C	N	24.2	–	
83:12	69	4	E	F?	20.3	–	
84:12	70	2	C	F	24.5	–	
85:12	71	2	E	F	20.7	–	
86:12	72	11	C	N?	22.55	.30	
87:12	73	6	C	N?	23.73	.16	
88:12	74	1	C	F?	25.2	–	
89:12	74	2	C	F?	25.3	–	
90:12	75–78	7	E	N?	20.43	.46	
91:12	75–78	36	E	F?	22.51	.21	13:4,14:4,15:4 ,16:4,17:4
92:12	76–78	1	C	F?	25.2	–	
93:12	76–78	1	C	F?	25.8	–	
94:12	78	3	C	F?	24.4	–	21:2,22:2,23:2
95:12	80	2	C	N?	23.4	–	

TABLE 1 (cont.)

ID	VLSR	AREA	C/E	N/F	⟨1⟩	r	COMMENTS
96:12	80	5	C	F?	23.44	.33	12:1,18:4
97:12	80	1	C	F?	23.8	–	
98:12	80	1	C	F?	25.6	–	
99:12	80	1	E	F?	26.0	–	
100:12	82	3	C	F?	24.73	–	25:2
101:12	83	22	E	F?	22.7	.55	
102:12	83	1	C	F?	23.8	–	
103:12	88	20	E	F	22.81	.33	22:4
104:12	89	1	C	F?	25.2	–	
105:12	89–90	3	C	N?	24.0	–	
106:12	90	1	C	F?	25.8	–	
107:12	92	15	E	N?	25.17	.16	
108:12	93	17	E	N?	23.51	.26	
109:12	95–98	52	E	F	23.84	.15	29:2,30:2,31:2, 32:2,23:4
110:12	105	10	E	N	22.56	.46	*
1:4	4	30	E	N	23.5		1:1
2:4	22	10	E	F	23.5		
3:4	22	2	E	F	23.5		
4:4	25	6	E	F	23.5		3:1,26:12
5:4	26	1	E	F	23.5		
6:4	29	1	C	F	23.5		
7:4	32	1	E	F	23.5		
8:4	34	1	E	F	23.5		
9:4	36	8	C	F	23.5		4:1,35:12
10:4	49	1	E	F	23.5		
11:4	53	22	E	N	23.5		8:1,18:2,60:12 *
12:4	62	30	E	N	23.5		10:1,74:12,81:12 *
13:4	73	7	E	N?	23.5		11:1,91:12 *
14:4	75	8	E	N?	23.5		91:12 *
15:4	76	2	E	F?	23.5		91:12 *
16:4	76	1	E	F?	23.5		91:12 *
17:4	77	2	E	F?	23.5		91:12 *
18:4	80	33	E	F?	23.5		12:1,96:12 *
19:4	85	5	E	F	23.5		
20:4	86	18	E	F	23.5		
21:4	87	2	E	F	23.5		
22:4	90	32	E	F	23.5		103:12 *
23:4	95	22	E	F	23.5		29:2,30:2,31:2, 32:2,109:12 *
24:4	102	21	E	F	23.5		13:1 *
25:4	106	17	E	N	23.5		13:1 *
26:4	110	2	E	F	23.5		*
27:4	115	10	E	F	23.5		15:1 *
28:4	120	2	E	F	23.5		"

TABLE 1 (cont.)

ID	VLSR	AREA	C/E	N/F	<1>	r	COMMENTS
1:2	2	2	C	F?	24.5		
2:2	6	50	E	N	24.5		
3:2	7	2	E	N	24.5		
4:2	13	7	E	F	24.5		
5:2	17	7	E	F	24.5		
6:2	19	1	E	F	24.5		
7:2	21	1	C	F	24.5		
8:2	22	7	E	F	24.5		
9:2	29	11	E	F	24.5		33:12 *
10:2	33	22	E	F	24.5		
11:2	35	5	E	F	24.5		36:12 *
12:2	36	2	C	F	24.5		36:12 *
13:2	38	1	E	F	24.5		
14:2	44	82	E	N	24.5		50:12 *
15:2	47	23	E	N?	24.5		58:12 *
16:2	48	25	E	N?	24.5		58:12 *
17:2	51	59	E	F?	24.5		59:12 *
18:2	54	71	E	N	24.5		8:1,11:4,60:12 *
19:2	62	27	E	F	24.5		75:12 *
20:2	65	3	C	F	24.5		
21:2	76	31	E	F?	24.5		94:12 *
22:2	76	4	E	F?	24.5		94:12 *
23:2	76	3	E	F?	24.5		94:12 *
24:2	79	5	E	F	24.5		
25:2	83	10	E	F?	24.5		100:12 *
26:2	85	6	E	F	24.5		
27:2	87	2	E	F	24.5		
28:2	88	57	E	F	24.5		
29:2	93	2	E	F	24.5		23:4,109:12 *
30:2	94	3	E	F	24.5		23:4,109:12 *
31:2	95	13	E	F	24.5		23:4,109:12 *
32:2	96	7	E	F	24.5		23:4,109:12 *
33:2	98	37	E	F	24.5		
34:2	101	1	E	F	24.5		*
35:2	103	2	C	F	24.5		*
36:2	103	2	E	F	24.5		*
37:2	106	48	E	F	24.5		*
38:2	107	13	E	F	24.5		*
39:2	111	3	E	F	24.5		*
40:2	112	1	E	F	24.5		*
41:2	114	57	E	F	24.5		*
42:2	119	4	E	F	24.5		*
43:2	121	2	C	F	24.5		*
44:2	124	1	C	F	24.5		*

TABLE 1 (cont.)

ID	VLSR	AREA	C/E	N/F	<1>	r	COMMENTS
1:1	4	47	E	N	23.5		1:4 *
2:1	11	10	E	N	23.5		
3:1	25	16	E	F	23.5		4:4,26:12 *
4:1	36	40	E	F	23.5		9:4,35:12 *
5:1	48	5	E	F	23.5		
6:1	50	17	E	F?	23.5		
7:1	52	5	E	F?	23.5		
8:1	52	3	E	N	23.5		11:4,18:2,60:12 *
9:1	58	20	E	N	23.5		
10:1	64	39	E	N	23.5		12:4,74:12 *
11:1	72	24	E	N?	23.5		13:4,91:12 *
12:1	80	45	E	F?	23.5		18:4,96:12 *
13:1	104	46	E	F	23.5		24:4,25:4 *
14:1	110	9	E	F	23.5		*
15:1	114	36	E	F	23.5		27:4 *

TABLE 2 Detailed Description of Cloud 4:4

T_{max}	12	8	4	0	4	8
12						
8		1	3	2	4	
4	4	3	1	4	3	
0	4					
−4	3					
−8	2					

V_{lsr}	12	8	4	0	4	8
12						
8		25	24	25	25	
4	25	26	(26)	26	23	
0	25					
−4	25					
−8	25					

TABLE 3a W_1

V	0–10	10–20	20–30	30–40	40–50	50–60	60–70	70–80	80–90	90–100	100–110	110–120
25.4	1.00	1.00	0.50	0.40	0.50	0.80	0.50	0.65	0.65	0.30	0.30	0.30
24.4	0.80	2.00	0.60	0.60	0.50	0.45	0.50	0.50	–	–	–	–
23.5	6.12	2.12	1.31	0.97	0.78	0.40	0.57	0.60	–	–	–	–
22.4	1.00	0.50	0.30	0.30	0.50	0.70	0.60	0.45	0.45	0.50	0.35	0.25
21.4	4.00	0.25	1.00	1.00	0.80	0.60	0.60	0.40	–	–	–	–
20.5	6.00	2.00	0.90	0.40	0.45	0.50	0.40	0.40	–	–	–	–

TABLE 3b W_2

25.4	0.20	0.18	0.15	0.15	0.20	0.20	0.12	0.12	0.20	0.15	0.20	0.20
24.4	0.15	0.15	0.20	0.30	0.10	0.15	0.15	0.10	–	–	–	–
23.5	0.16	0.17	0.15	0.15	0.15	0.15	0.21	0.18	–	–	–	–
22.4	0.20	0.15	0.15	0.15	0.15	0.20	0.20	0.20	0.20	0.20	0.20	–
21.4	0.15	0.15	0.20	0.15	0.15	0.20	0.15	0.15	–	–	–	–
20.5	0.20	0.15	0.08	0.15	0.20	0.20	0.20	0.15	–	–	–	–

TABLE 4a B_1

V	0–10	10–20	20–30	30–40	40–50	50–60	60–70	70–80	80–90	90–100	100–110	110–120
25.4	-1.00	-1.00	-1.00	0.00	0.00	0.00	-0.55	-0.50	-0.20	0.00	0.10	0.10
24.4	0.30	0.00	-0.60	-0.50	-0.10	-0.20	0.00	-0.60	–	–	–	–
23.5	0.00	0.00	0.00	-0.50	-0.50	-0.45	0.00	-0.25	–	–	–	–
22.4	-1.40	-1.50	-0.20	-0.5	-0.60	-0.60	-0.70	-0.50	0.10	-0.20	0.00	0.20
21.4	0.00	-0.90	-0.40	-0.50	-0.80	-0.70	-0.70	-0.25	–	–	–	–
20.5	0.00	0.00	0.00	-0.45	-0.80	-1.00	-0.50	-0.40	–	–	–	–

TABLE 4b B_2

25.4	-0.50	-0.18	0.05	–	0.40	-0.50	-0.30	-0.20	0.25	0.20	0.15	0.30
24.4	-0.65	–	–	0.00	-0.20	0.15	–	-0.05	–	–	–	–
23.5	0.20	0.00	0.20	0.00	-0.05	0.05	-0.30	-0.30	–	–	–	–
22.4	–	0.35	-0.35	0.35	-0.15	-0.30	-0.35	-0.10	0.10	0.20	-0.05	–
21.4	0.00	0.20	0.05	-0.30	-0.35	-0.40	-0.18	0.20	–	–	–	–
20.5	0.25	0.40	0.05	0.10	0.40	-0.05	0.00	0.10	–	–	–	–

TABLE 5a A_1

V	0–10	10–20	20–30	30–40	40–50	50–60	60–70	70–80	80–90	90–100	100–110	110–120
25.4	0.04	0.02	0.00	0.10	0.24	0.78	0.28	0.24	0.27	0.51	0.59	0.19
24.4	0.19	0.44	0.18	0.04	0.38	0.46	0.08	0.06	–	–	–	–
23.5	1.14	0.15	0.01	0.06	0.13	0.42	0.37	0.53	–	–	–	–
22.4	0.47	0.06	0.09	0.19	0.70	1.76	1.00	0.92	0.89	0.33	0.35	0.93
21.4	2.84	0.16	0.12	0.05	0.14	0.29	0.19	0.30	–	–	–	–
20.5	3.96	0.50	0.49	0.27	0.47	0.30	0.36	0.18	–	–	–	–

TABLE 5b A_2

25.4	0.17	0.05	0.07	0.00	0.17	0.12	0.11	0.10	0.04	0.42	0.37	0.31
24.4	0.05	0.00	0.00	0.26	0.44	0.06	0.08	0.15	–	–	–	–
23.5	0.02	0.04	0.10	0.06	0.12	0.18	0.27	0.25	–	–	–	–
22.4	0.01	0.17	0.02	0.01	0.41	0.82	0.39	0.72	1.46	1.51	0.94	–
21.4	0.03	0.18	0.13	0.23	0.17	0.03	0.10	0.06	–	–	–	–
20.5	0.04	0.11	0.10	0.08	0.04	0.23	0.12	0.26	–	–	–	–

TABLE 6 Comparison of log m and Neff for $v \leq 60$ and $v > 60$

α_{min}	-1.5	0.0	1.0	1.25	1.5	1.67	1.83	2.0	2.5
α_{max}	0.0	1.0	1.25	1.5	1.67	1.83	2.0	2.5	3.0
log m<60	-0.21	-1.21	-2.10	-1.87	-1.78	-2.13	-2.35	-3.03	-
log m>60	-	-	0.40	-1.74	-0.09	-0.15	-0.44	-0.97	-
$N_{<60}$	0	10	3	10	13	7	5	4	0
$N_{>60}$	0	0	14	0	11	12	7	7	0

REFERENCES

Allen, C.W. 1978, in Astrophysical Quantities, third edition, (London:Althone),p246

Appenzeller, I. 1971, A+A, 12, 313

1974, A+A, 36, 99

Baran, G.P. 1978, unpublished Ph.D. dissertation, Columbia University

Blaauw, A. 1964, Ann. Rev. Astr. Ap., 2, 213

Blitz, L. 1978, Ph.D. thesis, Columbia University

Blitz, L., and Shu, F.H. 1980, Ap.J., 238, 148

Bok, B.J. 1959, Observatory, 79, 58

Burton, W.B. 1971, A+A, 10, 76

Chandrasekar, S. 1969a, in Ellipsoidal Figures of Equilibrium, (New Haven:Yale), ch 6

1969b, ibid., ch 8

Cohen, R.S., Cong, H., Dame, T.M., and Thaddeus, P., 1980, in I.A.U. Symposium 87, Interstellar Molecules, ed. B. Andrew (Dordrecht:Reidel)

Cong, H.I. 1977, unpublished Ph.D. dissertation, Columbia University

Cowie, L.L., 1980, Ap.J., 236, 868

Disney, M.J., and Hopper, P.B., 1974, M.N.R.A.S., 168, 639

Elmegreen, B.G. 1979, Ap.J., 231, 372

Elmegreen, B.G., Lada, C.J., and Dickinson, D.F. 1979, Ap.J., 230, 415

Elmegreen, D.M., and Elmegreen, B.G. 1978, Ap.J., 220, 510

Gordon, W.B. and Burton, M.A. 1976, Ap.J., 207, L189

Heiles, C. 1976, Ann. Rev. Astr. Ap., 14, 1

Kazes, I. and Crovisier, J. 1980, in I.A.U. Symposium 87, Interstellar Molecules, ed. B. Andrew, (Dordrecht:Reidel)

Kutner, M.L., Tucker, K.D., Chin, G., and Thaddeus, P. 1977, Ap.J., 215, 521

Kwan, J., 1979, Ap.J., 229, 567

Lada, C.J., Elmegreen, C.G., Cong, H.I., and Thaddeus, P. 1978, Ap.J.L., 226, L39

Linke, R.A., and Wannier, P.G., 1974, Ap.J.L., 193, L41

Liszt, H.S., 1973, unpublished thesis, Princton University

Lynga, G. 1979, in I.A.U. Symposium 85, Star Clusters, ed. J.E. Hesser, (Dortrecht:Reidel), p 13

Masson, C. R. 1980, S. P. I. E. Proceedings, 231, 291

Mouscouvias, T.C. 1978, in Protostars and Planets, ed. T. Gehrels, (Tucson:Arizona), p 209

Norman, C., and Silk, J. 1980, Ap.J., 238, 158

Parker, E.N. 1966, Ap.J, 145, 811

Phillips, T.G., and Jefferts, K.B., 1973, Rev. Sci. Inst., 44, 1009

Roberts, W.W. 1969, Ap.J., 158, 123

Sato, F., Fukui, Y., and Hasegawa, T. 1980, in I.A.U. Symposium 87, Interstellar Molecules, ed. B. Andrew, (Dordrecht:Reidel)

Sargent, A.I. 1977, Ap.J., 218, 736

Shane, W.W. and Bieger-Smith, G.P. 1966, Bull. Astron. Inst. Neth, 18, 263

Solomon, P.M., Sanders, D.B. and Scoville, N.Z. 1979, in I.A.U. Symposium 84, The Large Scale Characteristics of the Galaxy, ed. W.B. Burton, (Dordrecht:Reidel), p 277

Stark, A.A., 1979, Ph.D. Dissertation, Princton University

Stark, A.A., and Blitz, L. 1978, Ap.J.L., 225, L15

Vrba, F.J. 1977, A.J., 82, 198

Vrba, F.J., Strom, S.E., and Strom, K.M. 1976, A.J., 81, 958

Westerhout, G. 1973, Maryland-Greenbank Galactic 21 cm Line Survey, third edition, (University of Maryland:College Park, Maryland)

Wilson, R.W., Jefferts, K.B., and Penzias, A.A. 1970, Ap.J.L., 161, L43

Woodward, P.R. 1978, in I.A.U. Symposium 84, The Large Scale Characteristics of the Galaxy, ed. W.B. Burton, (Dordrecht:Reidel), p 157

Woody, D.P., Phillips, T.G., Dolan, T.J., Miller, R.E. and Linke, R.A. 1981, IEEE Trans. on Magnetics, MAG-17, 84

Wootten, A. 1977, Ap.J., 216, 440

FIGURE CAPTIONS

Figure 1 — Definitions of the tilt angle τ and the apparent axial ratio r. Let aa be the longest chord joining two points on the outline of the cloud. The tilt angle τ is the acute angle between aa and the circle of constant galactic latitude through the center of aa. D is the length of aa and d is the length of the longest chord perpendicular to aa joining two points on the outline of the cloud. The axial ratio $r = D/d$.

Figure 2 — The viewing angle α is defined as the acute angle between the line of sight to the cloud and a line through the cloud center parallel to the nearest spiral arm. This is illustrated here for various possible locations of the cloud in the local spiral arms.

Figure 3 — Tilt angle τ plotted versus viewing angle α.

○ - clouds $\leq$ 40 pc long ● - clouds $>$ 40 pc long

Figure 4 — Axial ratio r plotted versus viewing angle α. The curves $U(\alpha)$ and $L(\alpha)$ are defined in the text.

○ - clouds $\leq$ 40 pc long ● - clouds $>$ 40 pc long

Figure 5 — Locations of the 1′, 2′, and 4′ grids.

Figure 6 — A section of the 4′ grid illustrating the analysis of the spectra into clouds. The box around each spectrum is

50 km s^{-1} wide and 10°K high. The darkened parts of the spectra represent cloud 4:4 in Table 1.

Figure 7 — Thickness of the molecular disk versus inverse kinematic distance. The solid line is the least squares line through the origin fitting the data. Its slope gives the thickness of the disk which is 44±11 pc. The dashed lines represent ± one standard deviations in the slope.

Figure 8 — Volume and normalizing kernals vs α for center clouds. The heavy lines in 8a and 8b show the volume kernal as functions of α for clouds 12:12 and 12:40 respectively. The heavy lines in 8c and 8d show the corresponding normalizing kernals. The light lines in all four parts of the figure show the mean values of the function over each bin. The vertical scales have been normalized to 1 in all cases, since the absolute scale does not affect the solution.

Figure 9 — Volume and normalizing kernals vs α for edge clouds. The heavy lines in 9a and 9b show the volume kernal as functions of α for clouds 12:4 and 12:18 respectively. The heavy lines in 9c and 9d show the corresponding normalizing kernals. The light lines in all four parts of the figure show the mean values of the function over each bin. The vertical scales have been normalized to 1 in all cases.

Figure 10 — Log μ versus α. The light line represents a power

law with index -0.72.

Figure 11 — The mass distribution. M(m) is the probability density per unit log m. It has been assumed that all clouds have the same (arbitrary) density, so that $m = A^3$.

FIGURE 1

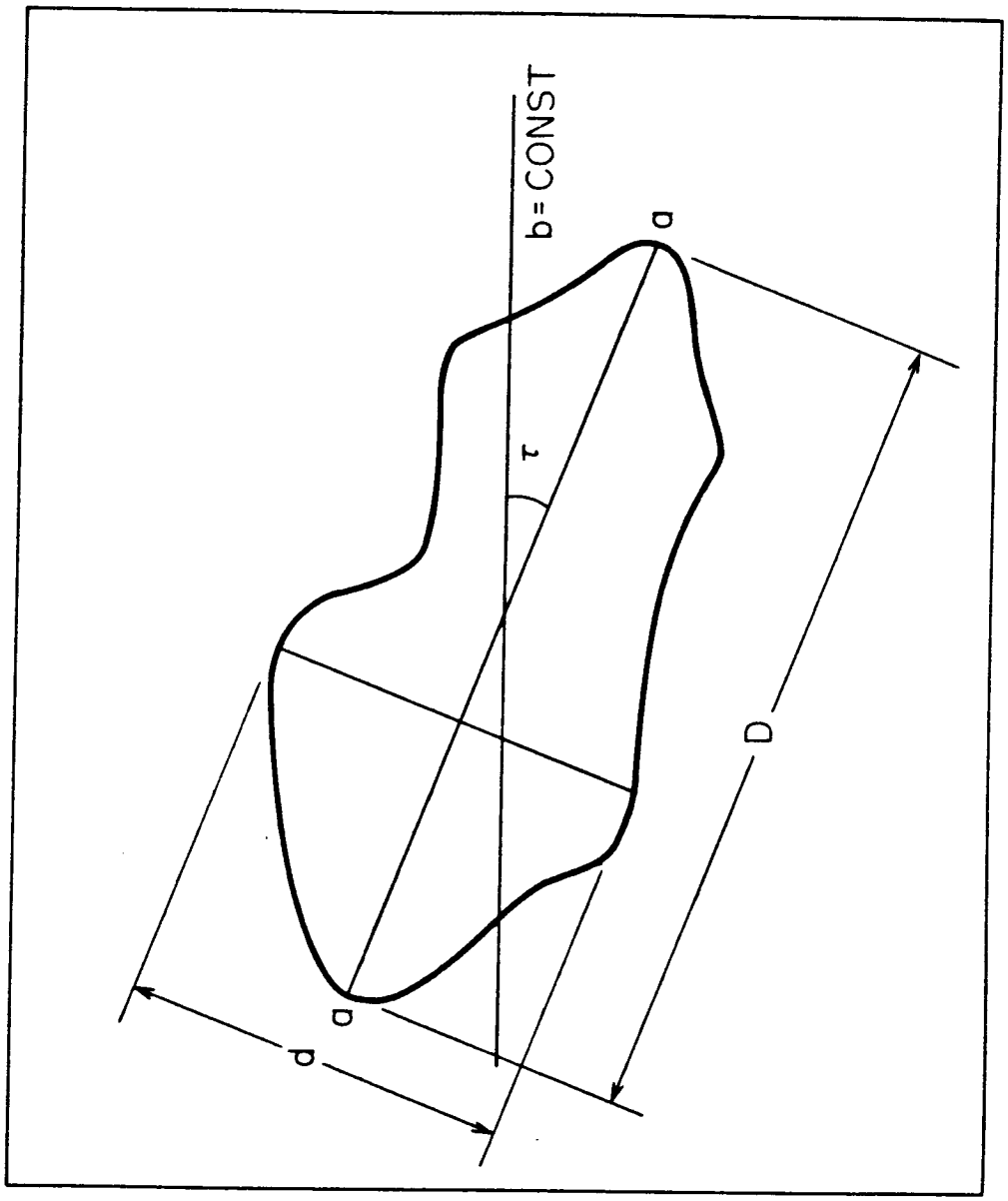

FIGURE 2

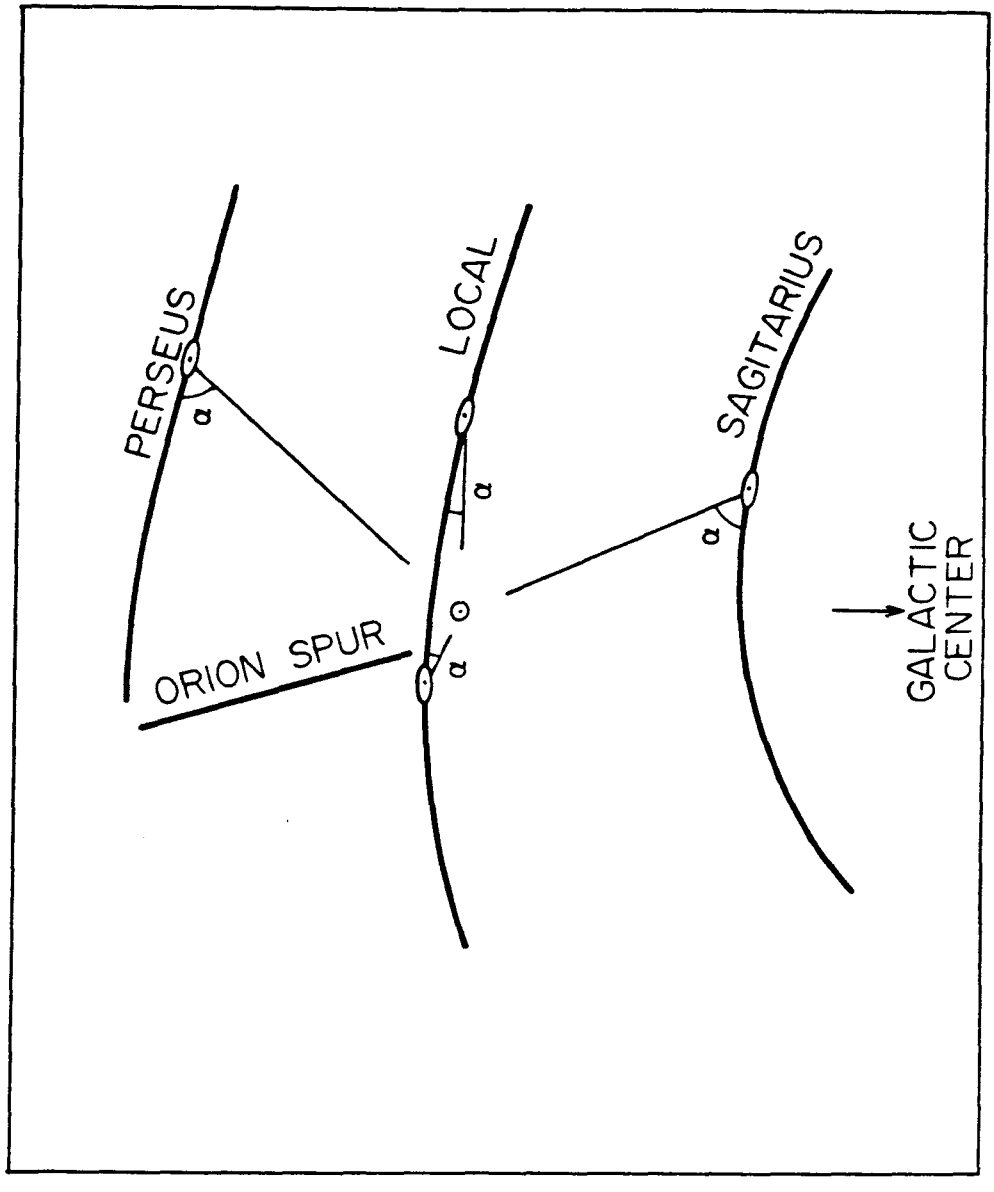

FIGURE 3

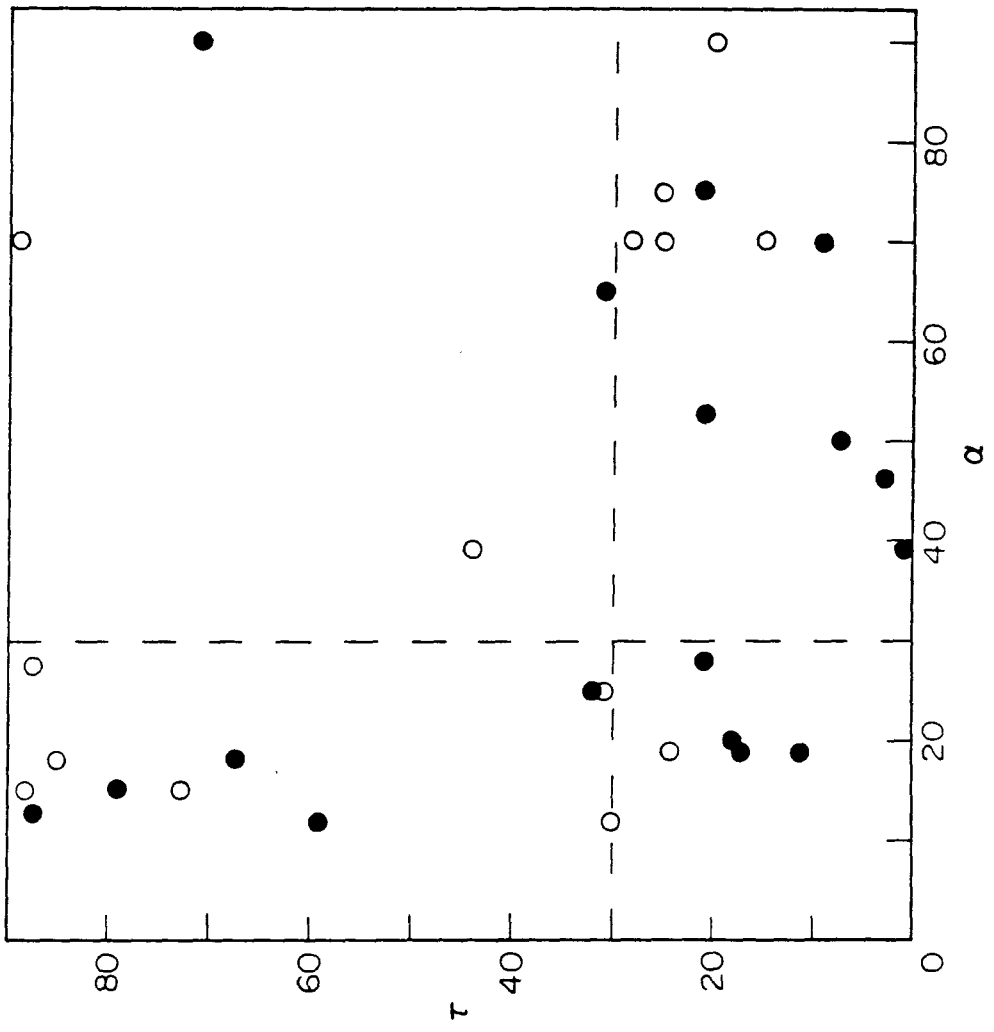

FIGURE 4

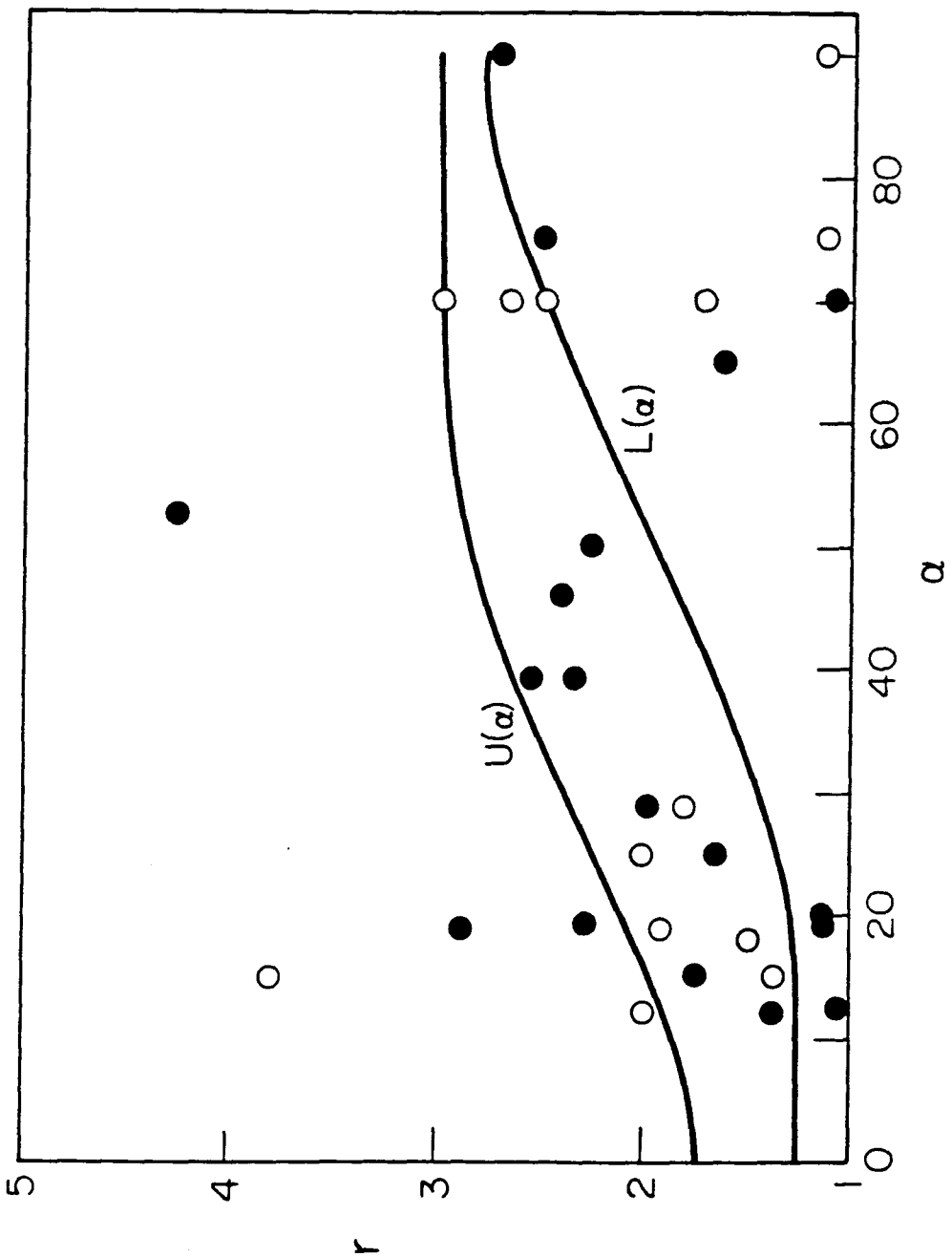

FIGURE 5

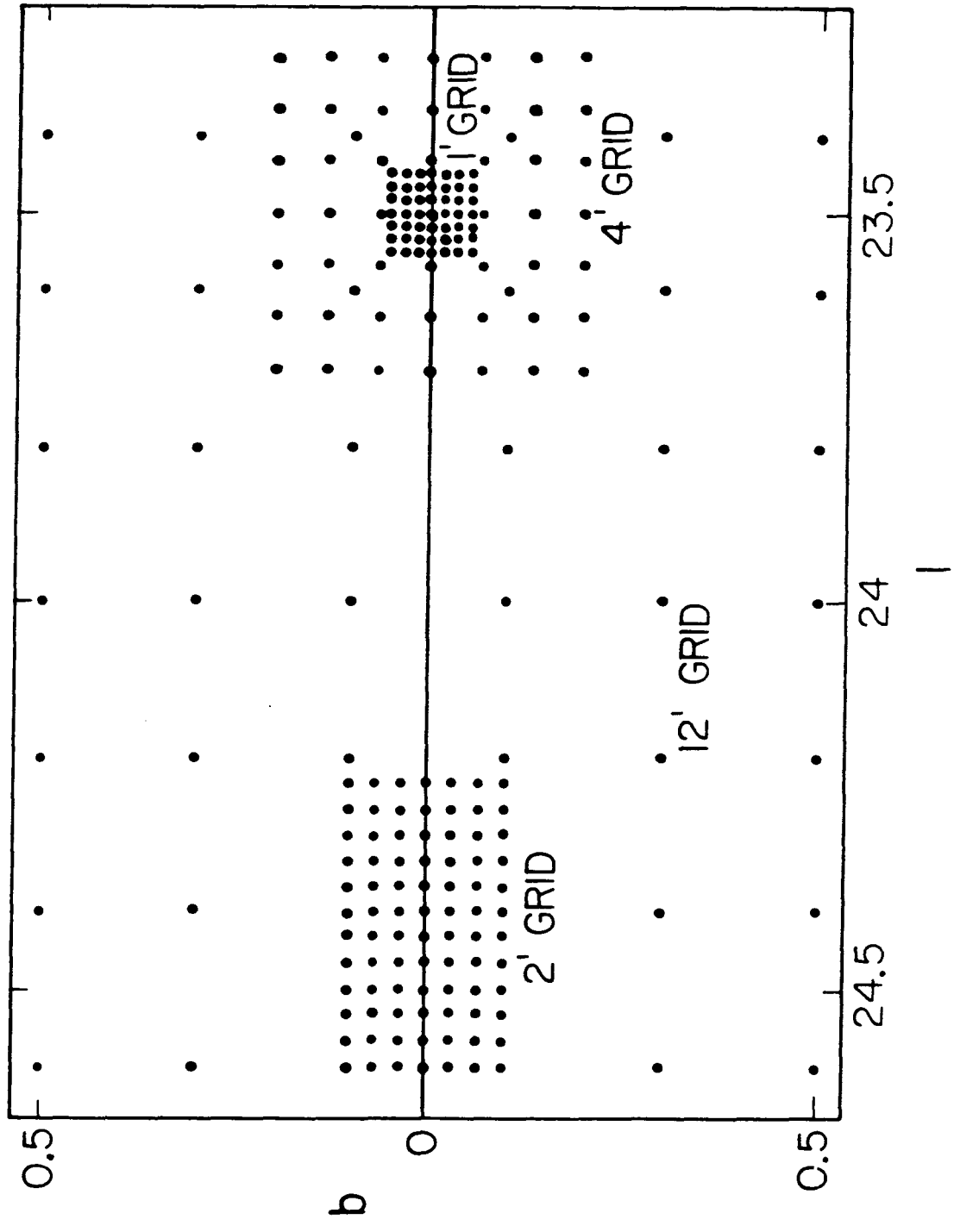

FIGURE 6

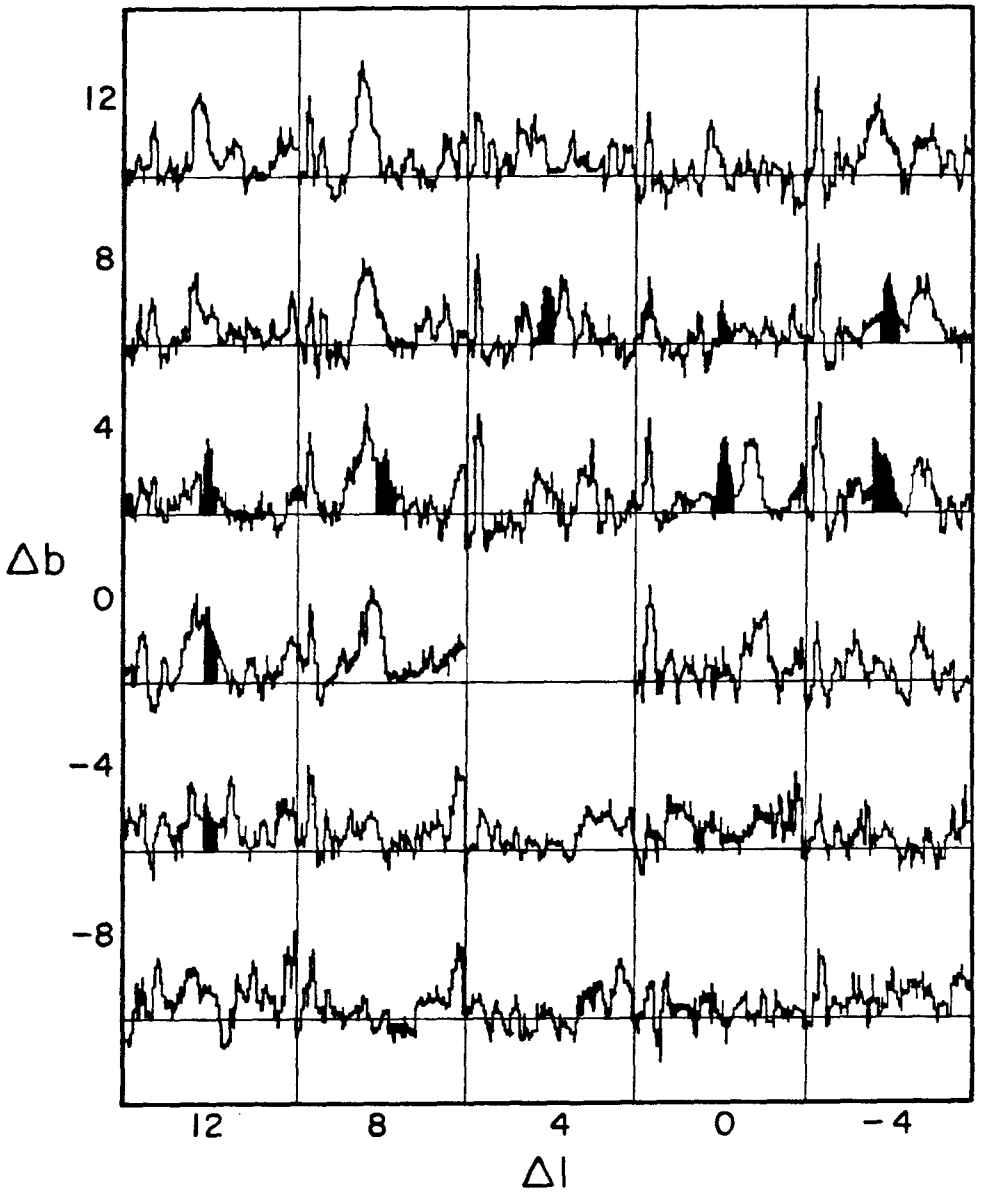

FIGURE 7

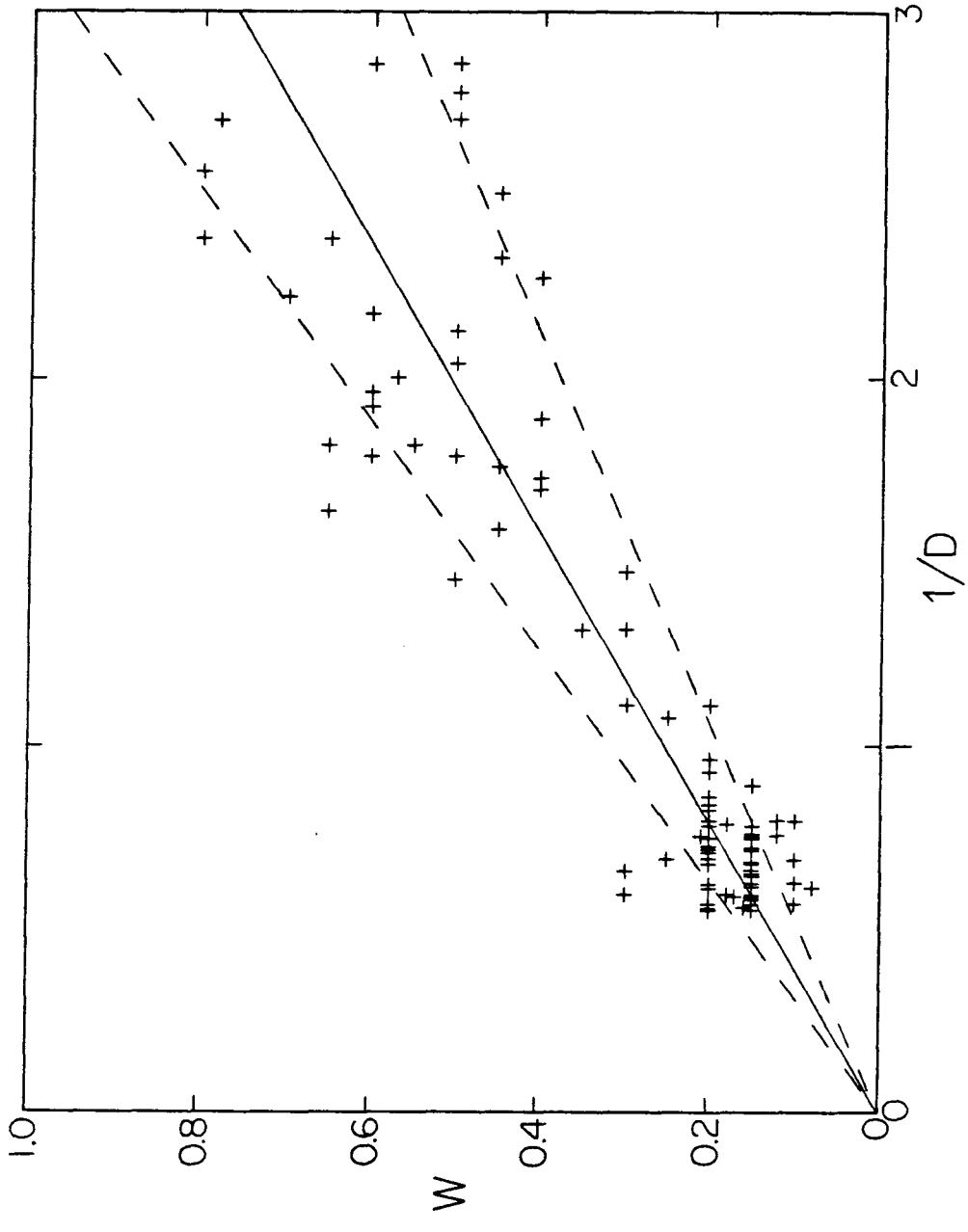

FIGURE 8

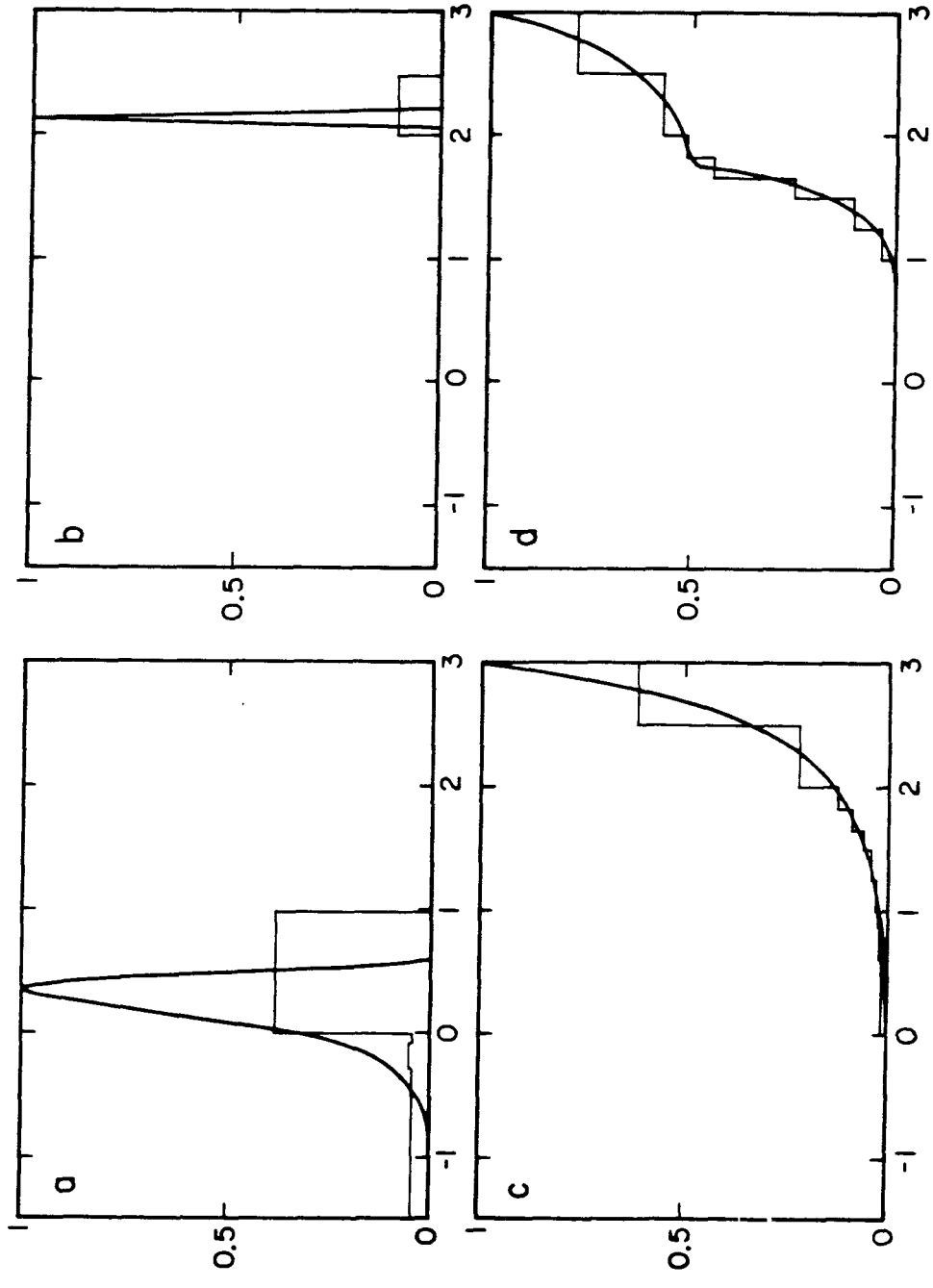

FIGURE 9

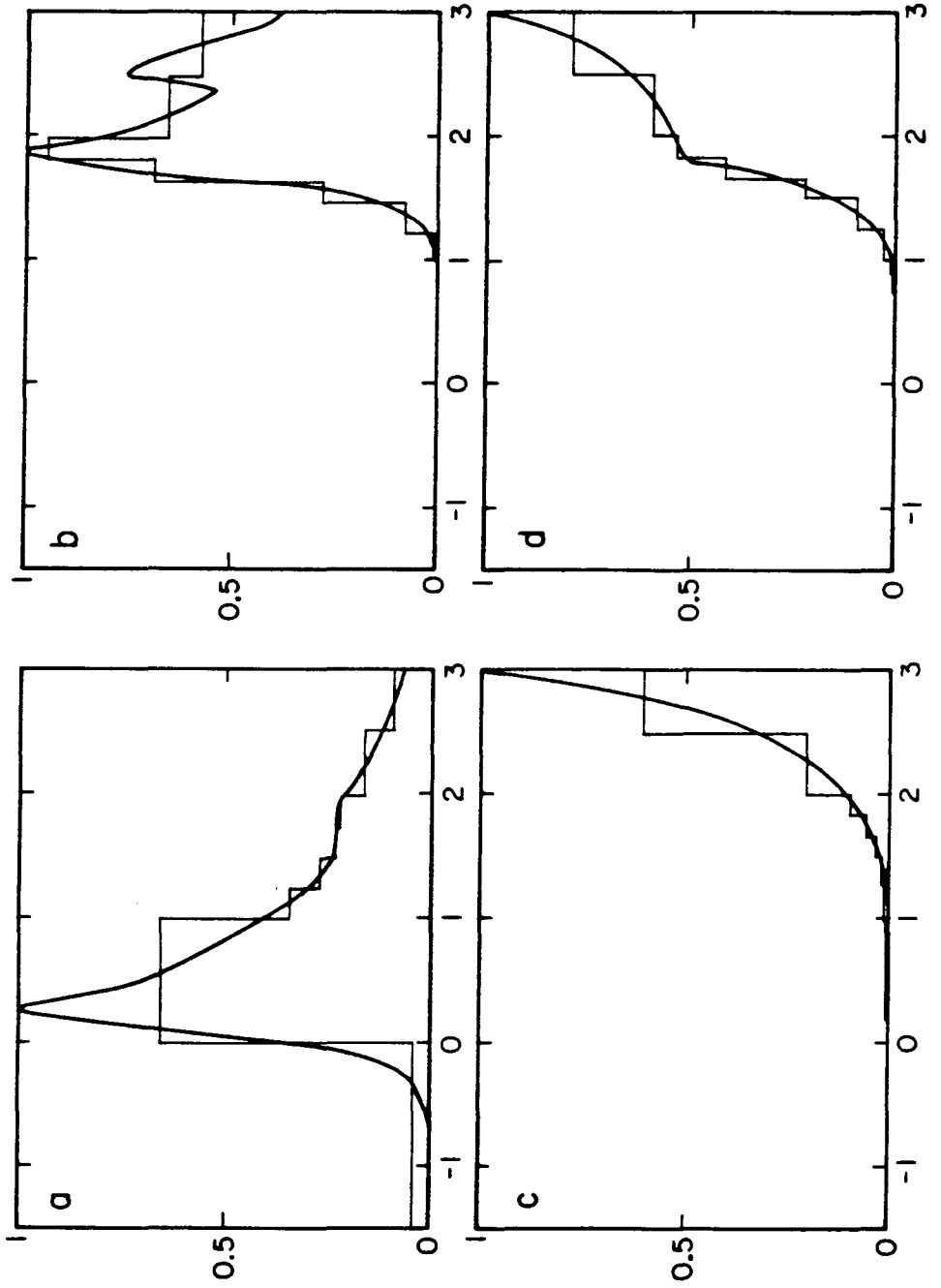

FIGURE 10

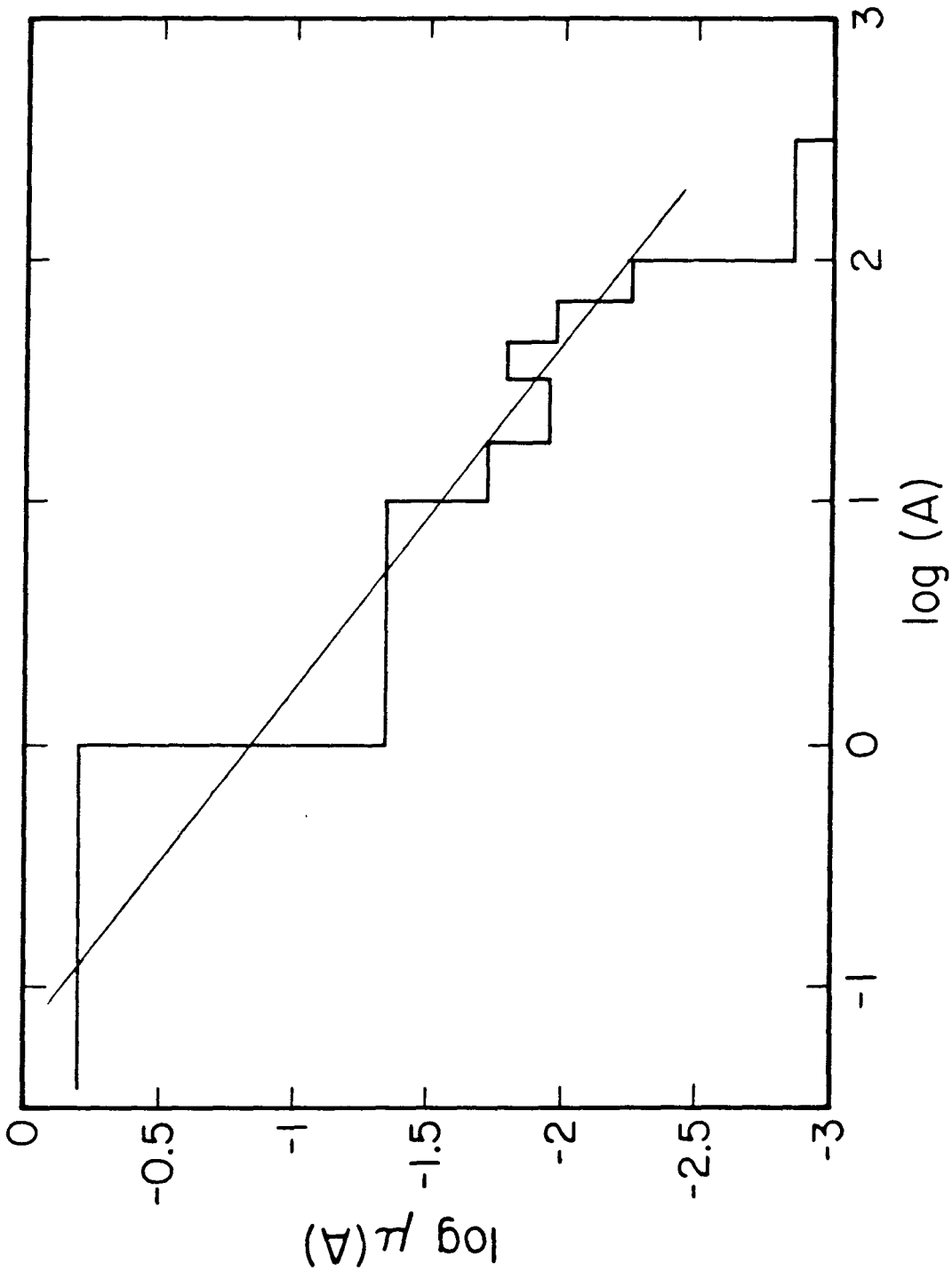

FIGURE 11